Study of the temperature dependence of the giant electric field-induced strain in Nb-doped BNT-BT-BKT piezoceramics

OBILOR, Uchechukwu, PASCUAL-GONZALEZ, Cristina, MURAKAMI, Shunsuke, REANEY, Ian and FETEIRA, Antonio <http://orcid.org/0000-0001-8151-7009>

Published version

OBILOR, Uchechukwu, PASCUAL-GONZALEZ, Cristina, MURAKAMI, Shunsuke, REANEY, Ian and FETEIRA, Antonio (2017). Study of the temperature dependence of the giant electric field-induced strain in Nb-doped BNT-BT-BKT piezoceramics. Materials Research Bulletin, 97, 385-392.

Study of the temperature dependence of the giant electric field-induced strain in Nb-doped BNT-BT-BKT piezoceramics

Uchechukwu Obilor[1], Cristina Pascual-Gonzalez[1], Shunsuke Murakami[2], Ian M. Reaney[2] and Antonio Feteira[1]

1. Christian Doppler Lab in Advanced Ferroic Oxides, Materials and Engineering Research Institute, Sheffield Hallam University, Howard Street, Sheffield, S1 1 WB, UK
2. Department of Materials Science and Engineering, The University of Sheffield, Mappin Street, Sheffield, S1 4JD, UK

Abstract

Dense $Bi_{0.487}Na_{0.427}K_{0.06}Ba_{0.026}TiO_3$ (BNKBT) and Nb-doped $Bi_{0.487}Na_{0.427}K_{0.06}Ba_{0.026}Ti_{0.98}Nb_{0.02}O_3$ (Nb-BNKBT) ceramics were prepared by the solid state reaction route. BNKBT is a non-ergodic relaxor and exhibits a piezoelectric response typical for a ferroelectric, whereas Nb-BNKBT is an ergodic relaxor and exhibits an electromechanical response typical for an incipient ferroelectric. The incorporation of 2 mol% of Nb into the BNKBT lattice is accompanied by an enhancement of the room-temperature unipolar field-induced strain from 0.19% to 0.43% at 75 kV/cm. BNKBT shows a depolarisation temperature of ~90°C, above which an electrostrictive response is observed, whereas Nb-BNKBT shows an electrostrictive response in the entire temperature range studied. At 40 kV/cm, Nb-BNKBT exhibits a temperature stable electromechanical response in comparison with undoped BNKBT, but it worsens under higher electric fields. These results may motivate further investigations on the impact of minor doping and driving electric fields on the electromechanical response of $Bi_{0.5}Na_{0.5}TiO_3$–$Bi_{0.5}K_{0.5}TiO_3$–$BaTiO_3$-based ceramics.

I-Introduction

Piezoelectric or electrostrictive actuators convert directly electrical energy into precisely controlled mechanical displacements. This valuable ability to control displacement is employed in many devices such as fuel injectors, micro-pumps, ink cartridges and medical instruments.[1] Currently, the market for piezoactuators is in excess of 20 billion dollars. Within some technological areas such as aerospace and automotive, temperature stability of the electromechanical response is a stringent pre-requisite. Currently, these actuators are invariably fabricated from $Pb(Zr,Ti)O_3$ (PZT)-based ceramics because of their large field-induced strain combined with also large electromechanical coupling coefficients for compositions lying at morphotropic phase boundary between rhombohedral and tetragonal symmetries. $Pb(Mg_{1/3}Nb_{2/3})O_3$ (PMN)-based electrostrictive ceramics can also show higher field-induced strains, with temperature stable electrostrictive coefficient, Q_{33}~ 0.023 m^4/C^2.

In the early 2000's, the European Union enacted legislation aiming at the elimination of toxic substances from electrical and electronic equipment to reduce their impact on the environment and health. This prompted a worldwide search for Pb-free piezoceramics. The investigation of Pb-free materials suitable for the fabrication of electromechanical actuators has been focused in the exploitation of different approaches, ranging from the search for systems exhibiting morphotropic phase boundaries to materials exhibiting electric field-induced phase transitions, such as incipient piezoelectrics.[2] The absence of remanent strain in incipient piezoceramics is accompanied by a so-called "giant" unipolar strain by comparison with conventional piezoceramics such as PZT, where the remanent strain due to non-180° domain switching only affords half of the maximum achievable strain under unipolar loading compared to bipolar loading.

Giant strain in Pb-free ceramics resulting from an electric field-induced phase was first measured by Zhang et al[3] for ceramics from the ternary $(Bi_{0.5}Na_{0.5})TiO_3$-$BaTiO_3$-$(K_{0.5}Na_{0.5})NbO_3$ (BNT-BT-KNN) system. Latterly, giant strains of the same origin were found in other BNT-based systems, with examples listed in Table I. A giant strain of ~0.87% under an applied electric field of 40 kV/cm was measured by Teranishi et al[4] in $Bi_{0.5}Na_{0.5}TiO_3$–$Bi_{0.5}K_{0.5}TiO_3$–$BaTiO_3$ (BNT-BKT-BT) tetragonal single crystals, along the [100] direction. This value is six times larger than that exhibit by PZT, which led several researchers to investigate the electromechanical response of ceramics in this ternary system. The large strain in BNT-based ceramics was shown to derive from a recoverable ergodic relaxor-to-normal ferroelectric state transition, due to small differences in the free energy between those two states under large applied electric fields. Some researchers investigated the impact of chemical doping on the electromechanical response of BNT-based systems. For example, Jo et al [5] found

donor Nb to muddle ferroelectric order in BNT-BT-KNN ceramics, leading to a decrease in the polarization and strain responses, whereas acceptor Fe-doping promoted ferroelectric stability with a concurrent increase in both polarization and strain responses.

Shieh et al [6] investigated the impact of Mn additions on the sinterability and electromechanical behaviour of $Bi_{0.487}Na_{0.427}K_{0.06}Ba_{0.026}TiO_3$ (BNKBT) ceramics. They found the induced electrostrain to decrease sharply from 0.14% to 0.05% when 2 mol% Mn was added to BNKBT. This detrimental effect of Mn doping contrasts dramatically with the improvement observed by the substitutional doping of Ti by 2 mol% Nb as shown in the present work. Basically, the substitution of Ti by 2 mol% Nb leads to an increase of the unipolar strain from 0.19% to 0.43% at 75 kV/cm. Moreover, Nb doping also enhanced the thermal stability of the electromechanical properties, leading to materials with potential application in actuators operating at least up to 100°C.

II-Experimental

$Bi_{0.487}Na_{0.427}K_{0.06}Ba_{0.026}TiO_3$ (BNKBT) and Nb-doped $Bi_{0.487}Na_{0.427}K_{0.06}Ba_{0.026}Ti_{0.98}Nb_{0.02}O_3$ (Nb-BNKBT) powders and ceramics were prepared by the conventional mixed oxide route. The starting materials were high-purity grade K_2CO_3, Na_2CO_3, Bi_2O_3, $BaCO_3$, Nb_2O_5, and TiO_2 powders (≥98%, ≥99.9%, 98%, 99.9% and ≥99% purity, respectively, Sigma-Aldrich). The starting chemicals were weighed in the required molar ratios and intimately mixed in propanol using a ball mill and zirconia media. The dried slurries were subsequently calcined in air at 850 °C. Their purity and crystallinity were determined by x-ray diffraction (XRD) using a high-resolution diffractometer (CuK_α, 1.5418 Å, D8 Empyrean XRD, PANalytical™, Almelo, The Netherlands) operated at 40 kV and 40 mA, in the 2Θ range between 20 and 80, with 2Θ increments of 0.013 and counting time of ~600 s per step.

The calcined powders were finely milled and uniaxially pressed into pellets under an applied pressure of ~150 MPa. These green compacts were fired in air at 1150 °C for 4 hours, using a controlled heating rate of 5 °C /min. Ceramic microstructures were examined using a scanning electron microscope (model: Quanta 200, FEI, Brno, Czech Republic) equipped with a W filament. Depolarized Raman spectra were obtained in back-scattering geometry using a micro-Raman spectrometer (Model InVia, Renishaw, New Mills, UK), equipped with a Rayleigh line-rejection edge filter that was set for the 532 nm excitation of an Ar^+ ion laser, which allowed ripple-free measurements down to 50 cm^{-1} from the laser line. Spectra were acquired using a 50× microscope objective and a laser power of 10 mW.

Pt-electrodes were applied to both sides of the fired ceramic disk for subsequent electrical measurements. Samples were poled at 80°C for 20 min under an electric field of 40 kV/cm. The small signal piezoelectric properties were measured by the Berlincourt method. The dielectric properties of both unpoled and poled ceramics were measured at 100 Hz, 1 kHz, 10 kHz, 100 kHz and 250 kHz from room-temperature to 580°C using a LCR meter coupled with a furnace. The electromechanical response was recorded using a ferroelectric tester (AixACCT TF 2000) by applying a high voltage triangular signal at a frequency of 1 Hz and measuring the strain using a laser interferometer. The large signal piezoelectric coefficient was calculated using the maximum achievable strain (S_{max}) normalized by the maximum electric field (S_{max}/E_{max}), where E_{max} is the maximum unipolar field. The ceramic microstructure were examined using a scanning electron microscope (SEM). Samples were gold coated before SEM to avoid charging.

III-Results and Discussion

(a) X-ray diffraction and Raman spectroscopy analyses

Room-temperature X-ray diffraction data for BNKBT and Nb-BNKBT ceramics fired at 1050°C for 4 h are illustrated in Fig. 1. Both ceramics appear to be single-phase within the detection limit of the technique. The replacement of Ti^{4+} by Nb^{5+} shifts the Bragg reflections towards lower angles, as clearly shown by the inset in Fig. 1 for (200). This indicates a small increase of the lattice volume, due to the larger ionic radii of Nb^{5+} (0.64 Å) in comparison with Ti^{4+} (0.605 Å). The inset also reveals rather symmetric reflections, i.e. without shoulders, normally indicative of a departure from cubic crystal symmetry. As shown later, both compositions exhibit a remarkable response to the application of an electrical field, corroborating a pseudocubic crystal structure, which is also supported for the appearance of strong Raman modes as illustrated in Fig. 2. Indeed, the presence of intense broad modes in the Raman spectra ceramic, provides compelling evidence that their local crystal symmetry cannot be described by the cubic $Pm\bar{3}m$ space group, as previously discussed by Pascual-Gonzalez et al [7]. The spectra can be divide into three regions, which correspond to different types of lattice vibrations. These regions were assigned according to the work of Schütz et al[8]. Hence, modes in the < 150 cm^{-1} region can be associated with A-site vibrations, thus involving Bi, Na, K and Ba cations, whereas modes in 150-450 cm^{-1} region can be associated with Ti–O vibrations, in particular with the bond strength. Finally, high-frequency modes above 450 cm^{-1} have all been associated with TiO_6 vibrations, namely the breathing and stretching of the oxygen octahedra. From

Fig. 2, it becomes apparent that Nb doping affects mainly modes associated with Ti–O and TiO_6 vibrations, which corroborates Nb incorporation in the B-site.

(b) Microstructural characterisation

The typical microstructures of BNKBT and Nb-BNKBT ceramics fired at 1050°C for 4 h are illustrated in Fig. 3.a and b, respectively. The microstructure of BNKBT ceramics consists mostly of submicron-sized cube-shaped grains as illustrated in Fig. 3.a. Although Nb-BNKBT ceramics also consist of cube-shaped grains, there appears to be two different grain size populations, as illustrated in Fig. 3.b.

(c) Room-temperature field-induced bipolar strain measurements

The room-temperature field-induced bipolar strain (S-E), polarisation (P-E) and switching currents (J-E) for BNKBT and Nb-BNKBT ceramics measured at 1 Hz under an applied electrical field of 75 kV/cm are illustrated in Fig. 4. BNKBT ceramics exhibit a so-called butterfly-shaped strain response with a maximum strain of ~0.20%, whereas Nb-BNKBT ceramics show sprout-shaped strain loops with negligible negative strain, reaching a maximum strain of ~0.42%, as illustrated in Fig. 4.a. The butterfly shaped-response, with a large negative strain (~0.09%) related to domain back switching is typical for ferroelectric materials. The drastic modification of the bipolar strain response from butterfly-shaped to a sprout-shaped upon Nb-doping suggests destabilisation of ferroelectricity at zero field.

Similarly, the polarisation curves, Fig. 4.b, show BNKBT ceramics to exhibit features typical for ferroelectrics, such as a large spontaneous polarization (P_s~42.3 $\mu C/cm^2$), remanent polarization (P_r~35 $\mu C/cm^2$) and coercive field (E_c ~34 kV/cm) alongside a sharp current peak (labelled P1, in Fig. 4.c) associated with ferroelectric domain switching when the applied electric field reaches E_c.

Interestingly, Nb-doping causes pinching of polarisation loop resulting in a significant decrease in P_r to ~ 7 $\mu C/cm^2$ and E_c to ~11 kV/cm, this is accompanied by the appearance of a small broad current peak at 34 kV/cm and an additional sharp peak at 53 kV/cm on electrical loading (labelled P2, in Fig. 4.c). The first current peak is associated to residual long-range ferroelectricity, whereas the second peak arises from a compositionally induced ferroelectric state. Upon electrical unloading, another peak (labelled as P3, in Fig. 4.c) appears at 6.5 kV/cm, which arises from domain back-switching. This clearly shows that the ferroelectric-induced order is not sustained in the absence of an applied

electric field. Recently, Guo et al[9] used *in-situ* transmission electron microscopy to show the disruption of ferroelectric domains into nanodomains at P3, while at P2 they observed coalescence and growth of nanodomains into large lamellar domains. Earlier, in $Bi_{0.5}Na_{0.34}K_{0.07}Ba_{0.06}TiO_3$ single-crystals, a peak in the switching current density accompanied by a jump in both polarisation and strain was reported near an applied electric-field of 20 kV/cm, but synchrotron experiments under an applied field as high as 40 kV/cm demonstrated that the crystal symmetry remained unchanged. Hence, Teranishi et al[4] postulated that giant strain in BNT-BKT-BT crystals arises from reversible switching of 90° domains. Back-switching of the 90° domains from a single domain state to a multidomain state was observed near 5 kV/cm.

In Fig. 4.b, the maximum achievable polarisation appears unaffected by doping, suggesting that although ferroelectric order in BNKBT is disturbed by chemical doping, the free energy of the ferroelectric phase is comparable to that of the relaxor phase, as discussed later, and ferroelectricity can be induced by an external electric field. Hence, the shape of polarisation loops clearly demonstrates ferroelectric order to be disturbed by Nb-doping, leaving a "weakly polar" phase with remanent polarisation of ~ 7 $\mu C/cm^2$ (at zero electric field), which by the application of an electric field can be reversibly transform into a ferroelectric phase, with a large spontaneous polarisation of ~ 42.3 $\mu C/cm^2$, a value similar to that of undoped BNKBT. In summary, the giant strain in Nb-BNKBT ceramics is a consequence of a reversible phase transition between a macroscopically "weakly" polar to a polar phase during electrical loading.

(d) Temperature dependent field-induced bipolar strain measurements

A further insight into the doping impact on the ferroelectricity in BNKBT can be gathered from in-situ temperature bipolar measurements provided in Fig. S1 and S2 of the supplementary information. At 25°C the P–E loop for undoped BNKBT ceramics shows typical ferroelectric features and those are retained as the temperature increases up to ~100°C. This is accompanied only by a moderate reduction in E_c, as illustrated in Fig. S1a. Above this temperature, there is a dramatic reduction in P_r and the loops become increasingly pinched with increasing temperature. This decrease in P_r is consistent with the disappearance of ferroelectric order and the appearance of an ergodic relaxor phase, as discussed later. In summary, a ferroelectric-to-relaxor phase transition occurs between ~100°C and ~125°C. A similar phenomenon was reported to occur at 108°C of the undoped BNKT ceramics.

The strain response of BNKBT in the 25 to 175°C temperature range also exhibits a dramatic transformation from a butterfly-shaped (typical for a ferroelectric) to a sprout-shaped (typical for a relaxor) response upon heating, as shown in Fig. S1b. This change is initially accompanied by an increase of the maximum achievable strain, and later by the simultaneous disappearance of the negative strain above 125°C and the emergence of a parabolic response which becomes slimmer and of smaller magnitude with increasing temperature. In contrast, both the polarisation and strain response of Nb-BNKBT show no dramatic changes, as shown in Fig. S2 of the supplementary information. The shape remains parabolic in the entire temperature range, similar to the response exhibited by BNKBT above 125°C. Hence, doping appears to shift the ferroelectric-to-relaxor transition down below room-temperature. Data in Fig. S1 and S2 show the coexistence of ferroelectric and relaxor phases to be revealed by pinch-shaped P-E loops and by sprout-shaped S-E loops. Moreover, they show this coexistence to be both temperature and compositionally dependent.

(e) Temperature dependence of the relative permittivity for poled and unpoled ceramics

Prior to further investigating this compositionally induced ferroelectric-to-relaxor transition, it is pertinent to recall that relaxors can exist in two different states, ergodic and non-ergodic, or a mix of both, due to different symmetries of the polar nanoregions (PNRs). For the purpose of this work, the difference between those two states can be rationalised as follows. A non-ergodic relaxor transforms irreversibly into the ferroelectric state under the application of a large electric field, whereas an ergodic transforms reversibly.[10] Basically, in an ergodic relaxor at room temperature, the application of a sufficiently large electric field can induce long-range ferroelectric order, which is only stable under electric field. Schutz et al[8] proposed the origin of non-ergodicity loss in BNT-based materials to be related to the breaking of Bi–O hybridization.

The distinction between those two states can be accomplished by the measurement of the dielectric properties of poled and unpoled ceramics. Fig. 5 shows the temperature dependence of relative permittivity (ε_r) and dielectric loss (tan δ) for BNKBT and Nb-BNKBT ceramics both unpoled and poled measured at 1, 10, 100 and 250 kHz. Unpoled specimens show strong frequency dispersion from room temperature up to ~200 °C for BNKBT (Fig. 5.a) and ~160°C for Nb-BNKBT (Fig. 5.b), which suggests that both specimens can be classified as relaxor ferroelectrics. Two distinct ε_r anomalies are visible in both compositions: a shoulder at ~130 °C (for BNKBT) and ~100 °C (for Nb-BNKBT) with considerable frequency dispersion and frequency-insensitive peaks at ~300 C. Nb-doping decreases the magnitude of ε_r.

In electrically poled BNKBT, a frequency independent dielectric anomaly appears as a discontinuity in ε_r and tan δ, as shown in Fig. 5.c. This anomaly is often referred to as depolarization temperature (T_d), but actually it is more correctly defined as the ferroelectric-to-relaxor temperature, T_{F-R}, i.e. the temperature at which field-induced ferroelectric order reverts back to an ergodic relaxor state. This anomaly is not detectable in poled Nb-BNKBT, as shown in Fig.5.d and such apparent absence is indicative that the substitution of Ti by 2 mol% Nb lowers T_{F-R} below room-temperature. Basically, BNKBT ceramics exhibit an electric-field response typical for a ferroelectric, however they are actually non-ergodic relaxors, which transform irreversibly into a ferroelectric state under the application of a high electric field, as shown in Fig. 4.a. Moreover, the single peak in the J-E loop, Fig. 4.c, for BNKBT ceramics implies an almost complete conversion into a ferroelectric state during electric field cycling. In contrast, the two current peaks exhibited by the J-E loops, Fig. 4.c, for Nb-BNKBT ceramics, suggest a two-step switching process, which first involves dissociation of ferroelectric domains followed by a compositionally induced ferroelectric state, this means also the coexistence of non-ergodic and ergodic phases. In summary, Nb-substitution lowers the ferroelectric-to-relaxor temperature, T_{F-R}, of BNKBT, and a giant strain emerges when T_{F-R} is below room temperature, as shown later in Fig. 6. Basically, the small difference in free energy between the relaxor and the ferroelectric states allows for a moderate electric field to convert a relaxor phase into a ferroelectric phase, resulting in large strain. Hence, Nb-BNKBT ceramics exhibit an electromechanical response typical for a so-called incipient ferroelectric. In the past, it has been reported that the addition of 2-3 mol% of dopants into BNT-BT and BNT-BKT ceramics is sufficient to induce incipient ferroelectricity. Nevertheless, Han et al observed that for Sn doping that amount increases to 5 mol%.

(f) Room-temperature field-induced unipolar strain measurements

In technological applications, only the positive field-induced strain is usable, hence the remainder of this work is focused on unipolar measurements of the electromechanical response of BNKBT and Nb-BNKBT ceramics. Room-temperature field-induced unipolar strain (S-E) and polarisation (P-E) for BNKBT and Nb-BNKBT ceramics measured at 1 Hz under an applied electrical field of 75 kV/cm are illustrated in Fig. 6. Undoped BNKBT ceramics exhibit a gradual increase of the strain and polarisation with increasing electric field reaching the maximum values of ~0.19 % and ~9.7 $\mu C/cm^2$ at 75 kV/cm, as shown in Fig. 6a and b, respectively. In contrast, Nb-BNKBT ceramics show an abrupt change of both strain and polarisation at ~ 45 kV/cm, as indicated by the arrow in Fig. 6. At greater applied electric fields, an almost linear response is observed, leading to a maximum strain of ~0.43 %

and a maximum polarisation of ~36 μC/cm^2 at 75 kV/cm. This behaviour is consistent with the saturation of the extrinsic contributions to the strain, and has been previously observed in other $Bi_{0.5}Na_{0.5}TiO_3$-based systems. For example, Acosta et al[11] found $0.75Bi_{0.5}Na_{0.5}TiO_3$-$0.25SrTiO_3$ ceramics to show a drastic change in strain at 30 kV/cm. It is now understood that such threshold fields mark a transition from a predominant relaxor state to a ferroelectric state, and these fields are often designated as E_{R-F}.

Small signal measurements of the piezoelectric coefficient, d_{33}, showed BNKBT ceramics to exhibit a d_{33} ~142 pC/N, which decreases dramatically to ~ 4 pC/N for Nb-BNKBT ceramics. This implies different origins for the electric field-induced strain in those two compositions. It is therefore interesting to evaluate the degree of hysteresis of the P-E loops by calculating the $\Delta S/S_{max}$ ratio, as the difference in the strain at $E_{max}/2$ normalized by S_{max}. $\Delta S/S_{max}$ was estimated to increase from 0.238 for undoped BNKBT ceramics to 0.462 for Nb-BNKBT ceramics. This quantification of the degree of hysteresis is often employed to provide a phenomenological description of the strain behaviour of incipient piezoceramics. Basically, the maximum achievable strain is inversely proportional to stability of the induced ferroelectric order, i.e. the larger the degree of instability in the field-induced ferroelectric order, larger the electric field-induced strain. Here, the $\Delta S/S_{max}$ ratio value for Nb-BNKBT ceramics is almost twice of that calculated for BNKBT, which is consistent with the different degrees of strain.

(g) Temperature dependent field-induced unipolar strain

Some of the large-volume applications of piezoceramics require strain over an extended temperature regime.[12] The usefulness of so-called high strain piezoceramics as materials for actuators is often impaired by the excessively large temperature dependence of the achievable strain. Hence, temperature dependent measurements of the unipolar strain for BNKBT and Nb-BNKBT ceramics were carried out to evaluate and compare the potential of those ceramics as actuator materials. Unipolar S-E and P-E measurements under applied fields of 40 kV/cm and 60 kV/cm are illustrated in Fig. 7 and 8 for BNKBT and Nb-BNKBT ceramics, respectively.

BNKBT ceramics exhibit abrupt changes in field-induced strain and polarisation with increasing temperatures, as illustrated in Fig. 7.a and b, respectively. Under an applied electric field of 40 kV/cm, the field-induced strain reaches a maximum of ~ 0.24% around 125 °C and a minimum value of ~0.10% at 25°C, as shown in Fig. 7.a. There is a dramatic change on the polarisation response at 125°C, as shown in Fig. 7.b. The maximum achievable polarisation shows a moderate temperature

dependence above 125°C with values around 30 μC/cm^2. Similarly, under an applied electric field of 60 kV/cm, both field-induced strain and polarisation exhibit a larger temperature dependence. A maximum strain of 0.37% is reached at 100°C, as shown in Fig. 7.c, whereas the maximum polarisation reaches ~35 μC/cm^2, as shown in Fig. 7.d. Also at 100°C, a change in the slope in both the S-E loops and P-E loops takes place at an applied electric field of ~28 kV/cm, as indicated by the arrow. This arises due to the evolution of a relaxor to a ferroelectric state.

In contrast, Nb-BNKBT ceramics under an applied field of 40 kV/cm, exhibit a much lower temperature dependence of the electromechanical properties, as illustrated in Fig. 8. The maximum unipolar strain at room-temperature is ~0.13%, it increases slightly to ~0.14% at 50 °C, remaining around this value up to 100 °C, above each it decreases gradually down to ~0.11% at 175°C, as illustrated in Fig. 8.a. The maximum unipolar polarisation is rather stable over the entire temperature range, as shown in Fig. 8.b. Nevertheless, a different picture of the temperature dependence is observed for Nb-BNKBT ceramics under an applied field of 60 kV/cm, as shown in Fig. 8c and d. At this higher field, the strain drops from 0.375% at 25°C to 0.187% at 175°C. In this case, a change in the slope in both the S-E loops and P-E loops takes place at an applied electric field of ~52 kV/cm, as indicated by the arrow, but at much lower temperatures. The temperature variation of the polarisation and strain for BNKBT and Nb-BNKBT measured at 40 and 60 kV/cm is illustrated in Fig. 9. Nb-BNKBT ceramics exhibit the largest temperature stability when measured at 40 kV/cm. Under this field the variation of strain is no greater than 20% in the entire temperature range. In comparison, undoped BNKBT ceramics will undergo a change in strain greater than 20% on the first 75 °C. Nevertheless, the temperature dependence of the strain for Nb-BNKBT increases dramatically under an applied field of 60 kV/cm, as shown in Fig. 9.b.

In fig. S3 of the supplementary material, measurements at 5 different applied fields showed BNKBT ceramics (Fig. S3a) to exhibit similar temperature of the field induced strain. In contrast, the temperature dependence of the field induced strain for Nb-BNKBT ceramics (Fig. S3b) increases monotonically with increasing electric field.

Interestingly, the temperature dependence of the unipolar J-E loops for BNKBT and Nb-BNKBT, exhibit distinctive behaviours as shown in Fig. S4 of the supplementary material. The most remarkable difference concerns the peak maxima for the current. In undoped, BNKBT ceramics, a current peak emerges at 100°C at a loading field of ~25 kV/cm. This peak shifts to higher fields with increasing temperature but reduces in intensity until it virtually disappears at 175°C. On unloading, the current peak at 100°C appears only when the applied electric field is lowered to ~1.5 kV/cm, and again it increases to higher fields with increasing temperature. In contrast, for Nb-BNKBT ceramics

peaks in the J-E loops are only visible up to 50°C and appear at much larger fields in comparison with undoped BNKBT ceramics. These peaks have similar origins, but they appear in different temperature regimes, because the relaxor-to-ferroelectric is compositionally dependent.

IV-Conclusions

A non-ergodic relaxor with the nominal composition $K_{0.06}Bi_{0.487}Na_{0.427}Ba_{0.026}TiO_3$ was transformed into an ergodic relaxor by chemical substitution of Ti by 2 mol % Nb. The doped material exhibits a giant unipolar strain of 0.43% (S_{max}/E_{max} =573 pm/V) at room-temperature under applied electric field of 75 kV/cm. The average crystal structure of BNKBT remains unaltered by the incorporation of Nb, however the electromechanical response changes dramatically, because a relaxor-to-ferroelectric transition is brought down below room-temperature. At an applied electric field of 40 kV/cm, the doped material shows a variation of the induced strain no greater than 20% in the 25-170 °C temperature range, however this is accompanied by modest maximum strain of 0.13%. This observation shows how temperature stability of the electromechanical response can be strongly dependent of the driving electrical fields.

Acknowledgments

Mr S. Creasey is acknowledged for support with the SEM imaging. Ian M. Reaney and Shunsuke Murakami acknowledge the support of EP/L017563/1. Antonio Feteira acknowledges Sheffield Hallam University's strategic research infrastructure funding for the purchase of the Piezoelectric measurement system used in this work.

References

1. J. Rodel, K. Webber, R. Dittmer, W. Jo, M. Kimura and D. Damjanovic, *Journal of the European Ceramic Society*, 2015, **35**, 1659-1681.
2. S. Zhang, A. Kounga, W. Jo, C. Jamin, K. Seifert, T. Granzow, J. Rodel and D. Damjanovic, *Advanced Materials*, 2009, **21**, 4716-+.
3. S. Zhang, A. Kounga, E. Aulbach, H. Ehrenberg and J. Rodel, *Applied Physics Letters*, 2007, **91**.
4. S. Teranishi, M. Suzuki, Y. Noguchi, M. Miyayama, C. Moriyoshi, Y. Kuroiwa, K. Tawa and S. Mori, *Applied Physics Letters*, 2008, **92**.
5. W. Jo, E. Erdem, R. Eichel, J. Glaum, T. Granzow, D. Damjanovic and J. Rodel, *Journal of Applied Physics*, 2010, **108**.
6. J. Shieh, Y. Lin and C. Chen, *Journal of Physics D-Applied Physics*, 2010, **43**.
7. C. Pascual-Gonzalez, G. Schileo, A. Khesro, I. Sterianou, D. Wang, I. M. Reaney and A. Feteira, *Journal of Materials Chemistry C*, 2017, 1990-1996.

8. D. Schutz, M. Deluca, W. Krauss, A. Feteira, T. Jackson and K. Reichmann, *Advanced Functional Materials*, 2012, **22**, 2285-2294.
9. H. Z. Guo, X. M. Liu, F. Xue, L. Q. Chen, W. Hong and X. L. Tan, *Physical Review B*, 2016, **93**.
10. W. Jo, S. Schaab, E. Sapper, L. Schmitt, H. Kleebe, A. Bell and J. Rodel, *Journal of Applied Physics*, 2011, **110**.
11. M. Acosta, W. Jo and J. Rodel, *Journal of the American Ceramic Society*, 2014, **97**, 1937-1943.
12. A. Khesro, D. W. Wang, F. Hussain, D. C. Sinclair, A. Feteira and I. M. Reaney, *Applied Physics Letters*, 2016, **109**, 142907.
13. K. Seifert, W. Jo and J. Rodel, *Journal of the American Ceramic Society*, 2010, **93**, 1392-1396.
14. C. G. Ye, J. G. Hao, B. Shen and J. W. Zhai, *Journal of the American Ceramic Society*, 2012, **95**, 3577-3581.
15. K. Wang, A. Hussain, W. Jo and J. Rodel, *Journal of the American Ceramic Society*, 2012, **95**, 2241-2247.
16. W. F. Bai, J. H. Xi, J. Zhang, B. Shen, J. W. Zhai and H. X. Yan, *Journal of the European Ceramic Society*, 2015, **35**, 2489-2499.

List of Figures

Table I. Room-temperature maximum achievable strain for some Pb-free piezoceramics.

	Strain (%)	S_{max}/E_{max} (pm/V)	Electric Field (kV/cm)	Sample nature
92BNT-6BT-2KNN[3]	0.45	560	80	Random polycrystalline
91BNT-6BT-3KNN[5]	~0.40	~500	80	Random polycrystalline
92BNT-6BT-3KNN 1 at% Fe (acceptor)[5]	~0.45	~560	80	Random polycrystalline
91BNT-6BT-3KNN 1 at% Nb (donor)[5]	~0.27	~338	80	Random polycrystalline
79.2BNT-19.83BKT-0.97KNN[13]	0.48	600	80	Random polycrystalline
79BNT-20BKT-1KNN[14]	0.45	750	60	Template grain growth
76BNT-19BKT-5ST[15]	0.36	600	60	Random polycrystalline
BNT-BKT-6BT[4]	0.87	2175	40	Single crystal
BNT-BKT-5BT[16]	0.32	710	45	Template grain growth
85.4BNT-12BKT-2.6BT[6]	0.14	295	50	Random polycrystalline
85.4BNT-12BKT-2.6BT 2 mol% Mn[6]	0.06	84	50	Random polycrystalline
85.4BNT-12BKT-2.6BT [This work]	0.19	230	75	Random polycrystalline
85.4BNT-12BKT-2.6BT 2 mol% Nb (donor) [This work]	0.43	573	75	Random polycrystalline

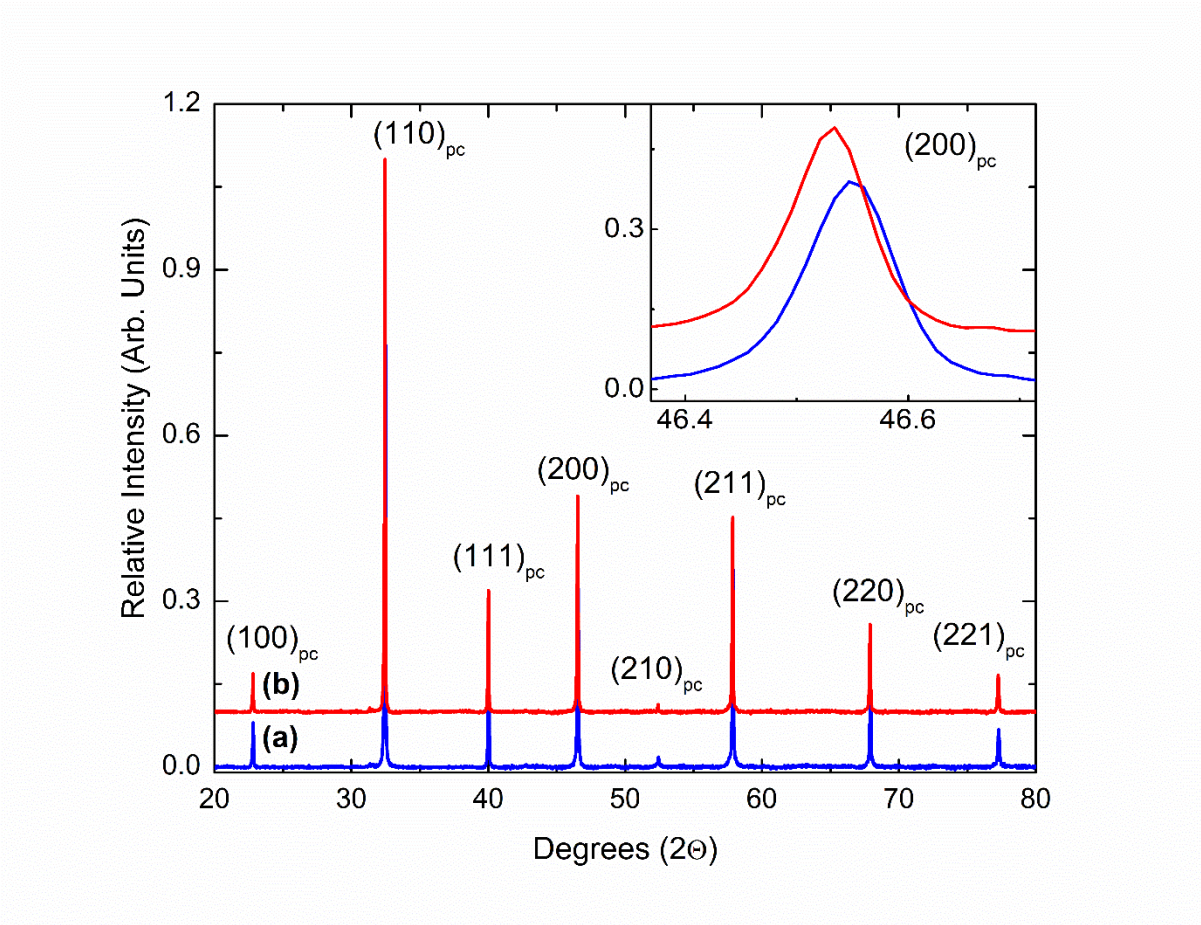
1.2
0.9
0.6
0.3
0.0
Relative Intensity (Arb. Units)
20
30
40
50
60
70
80
Degrees (2Θ)
(110)pc
(200)pc
(111)pc
(211)pc
(220)pc
(221)pc
(100)pc
(210)pc
(b)
(a)
0.3
0.0
46.4
46.6

Fig 1

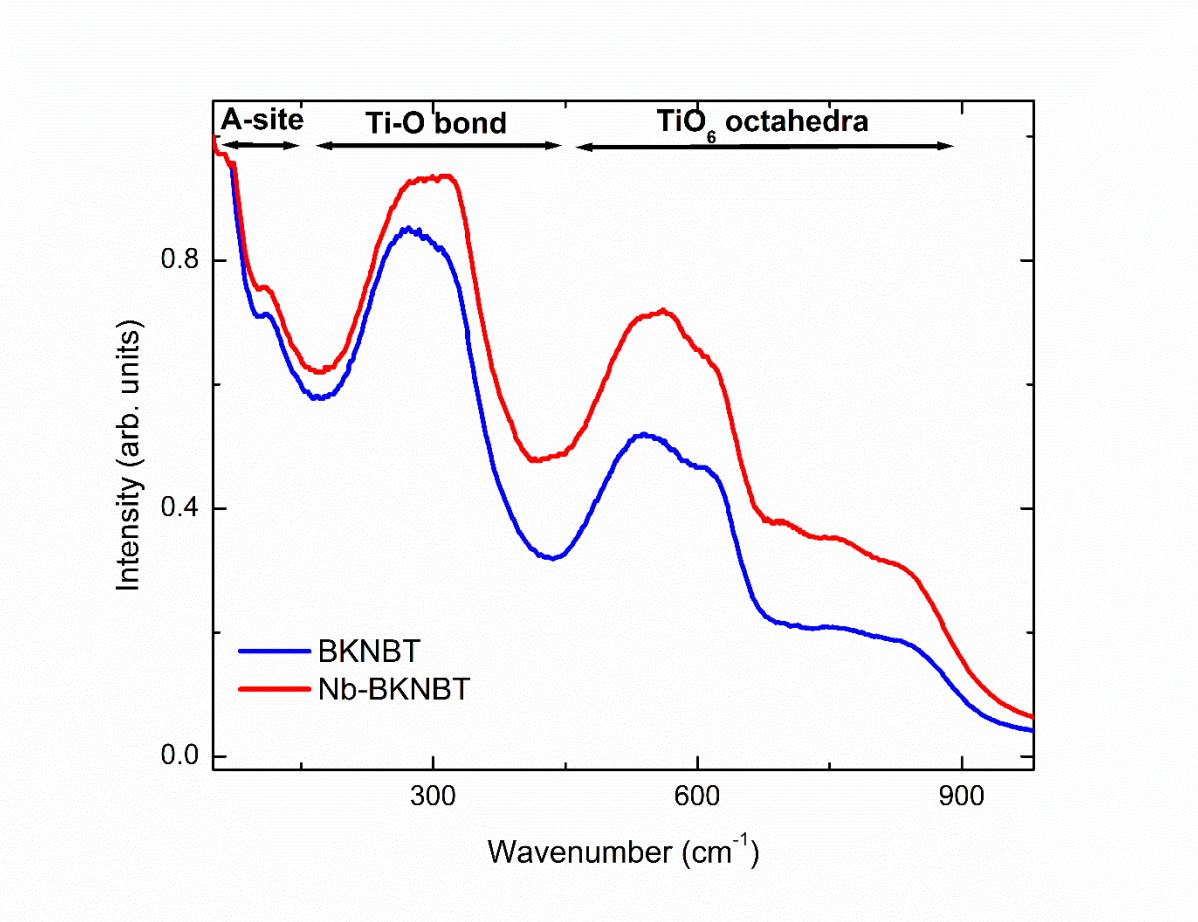
A-site
Ti-O bond
TiO6 octahedra
0.8
0.4
0.0
Intensity (arb. units)
BKNBT
Nb-BKNBT
300
600
900
Wavenumber (cm-1)

Fig. 2

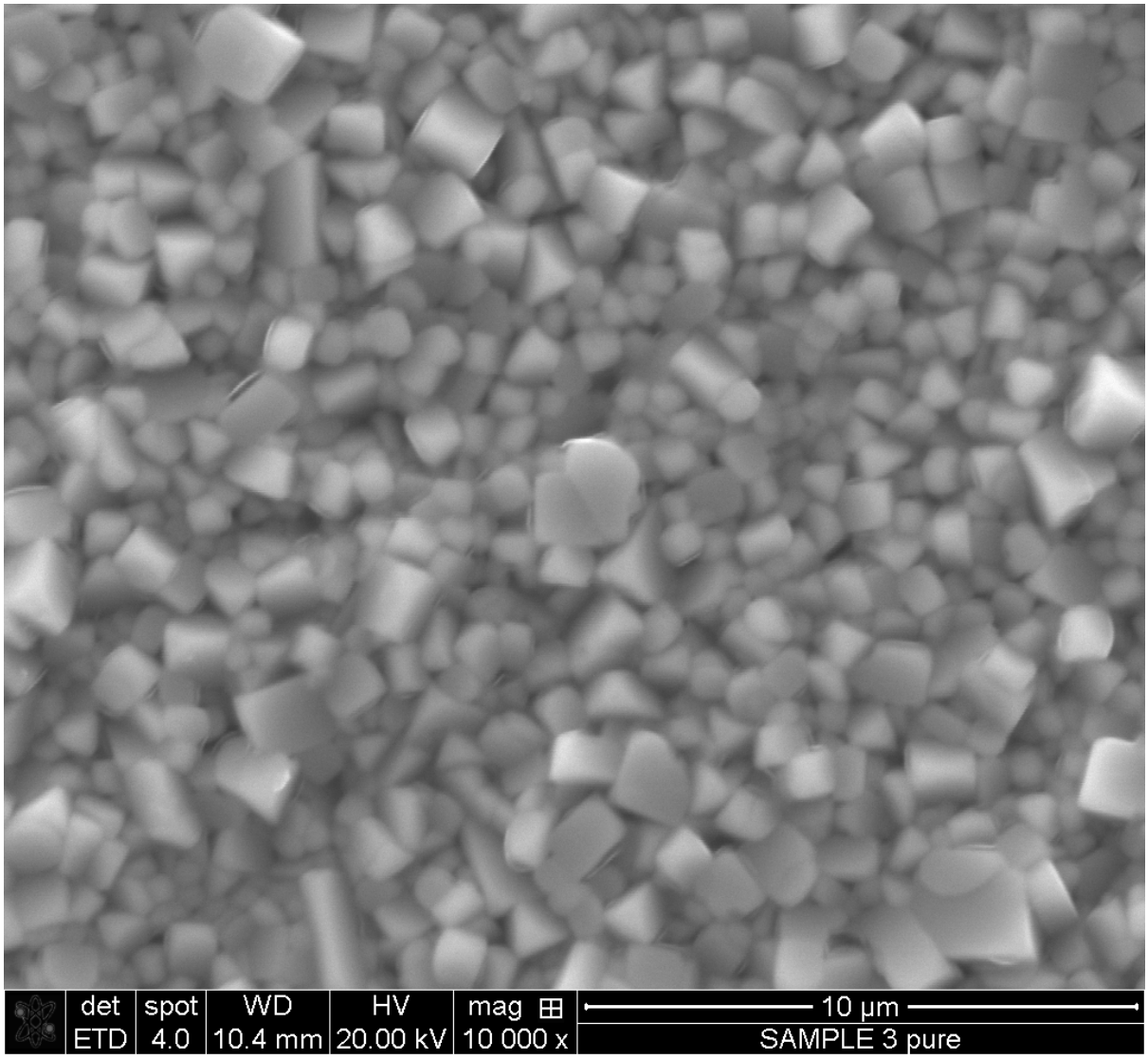
det
ETD
spot
4.0
WD
10.4 mm
HV
20.00 kV
mag
10 000 x
10 µm
SAMPLE 3 pure

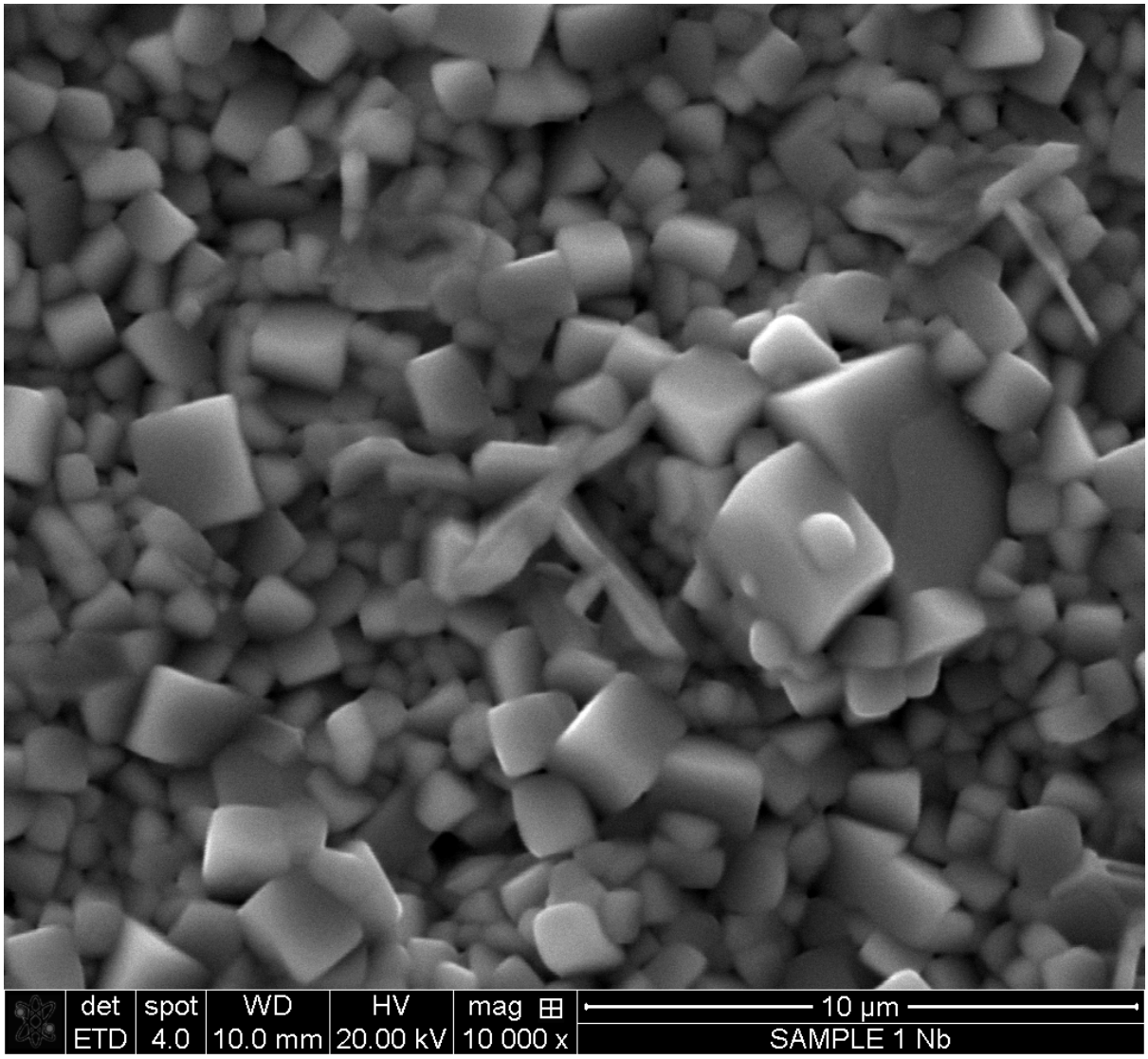

Fig. 3

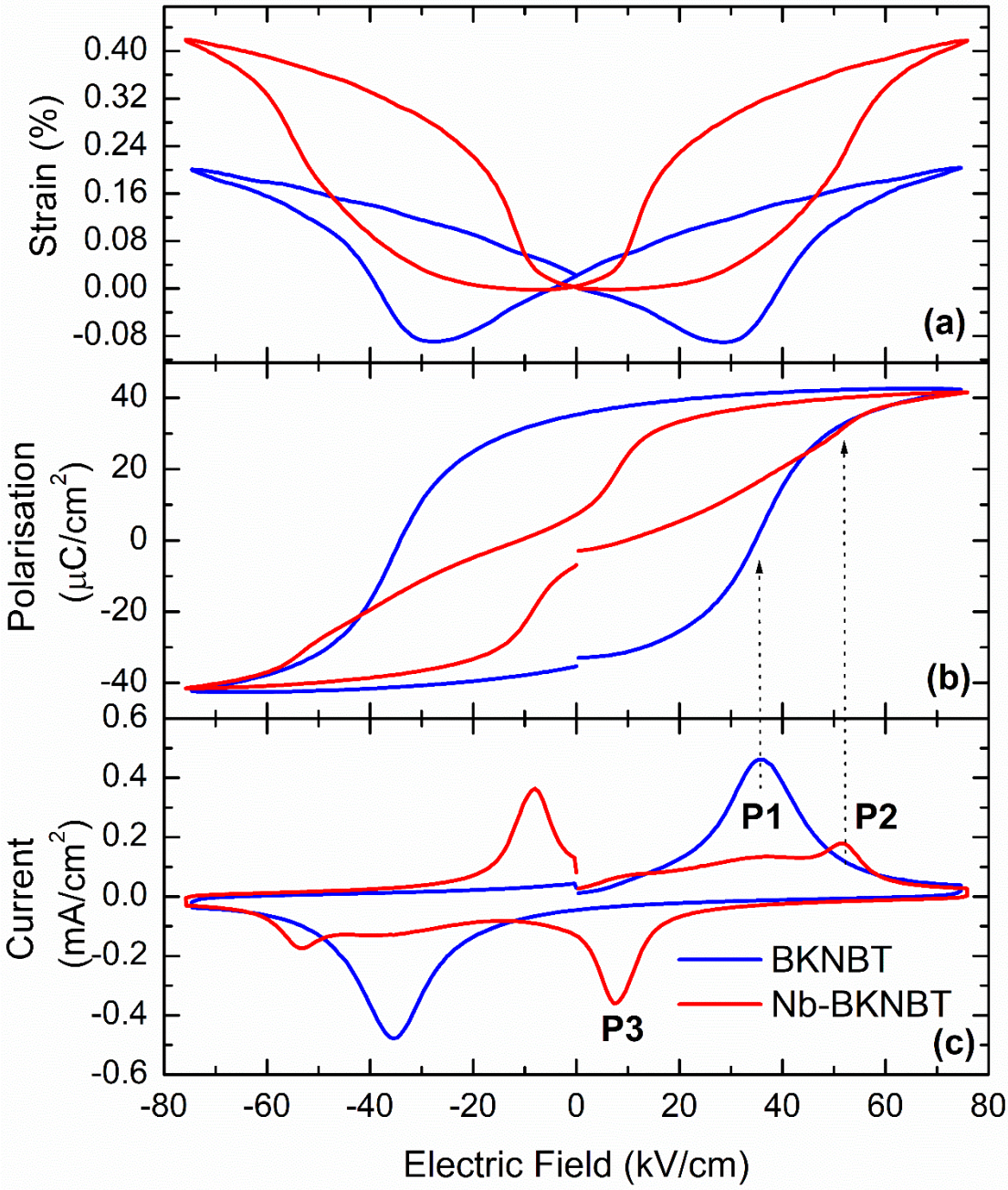
Strain (%)
0.40
0.32
0.24
0.16
0.08
0.00
-0.08
(a)
Polarisation (μC/cm²)
40
20
0
-20
-40
(b)
Current (mA/cm²)
0.6
0.4
0.2
0.0
-0.2
-0.4
-0.6
P1
P2
P3
BKNBT
Nb-BKNBT
(c)
-80
-60
-40
-20
0
20
40
60
80
Electric Field (kV/cm)

Fig. 4

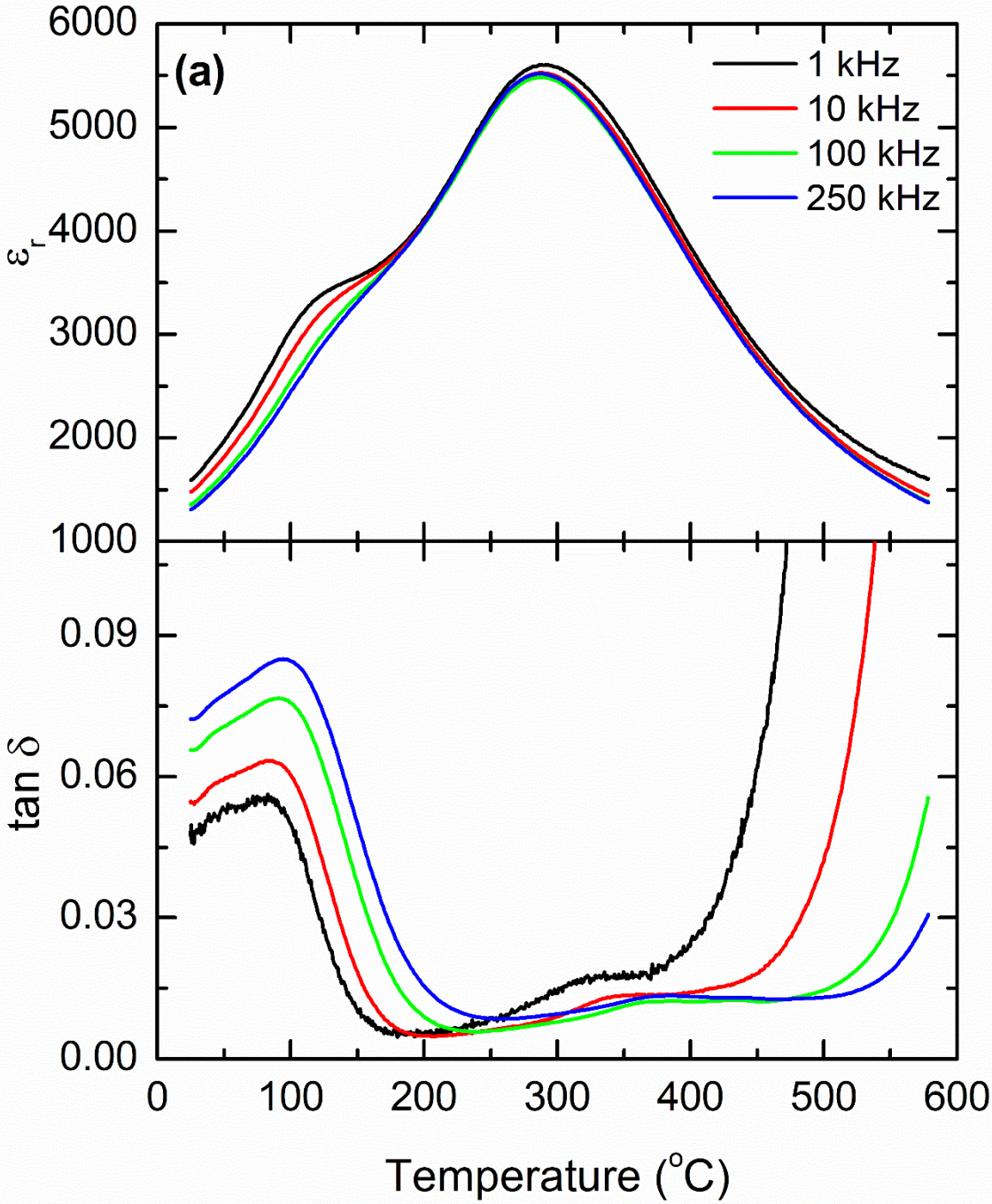
(a)
1 kHz
10 kHz
100 kHz
250 kHz
ε_r
6000
5000
4000
3000
2000
1000
tan δ
0.09
0.06
0.03
0.00
0
100
200
300
400
500
600
Temperature (°C)

Fig5a

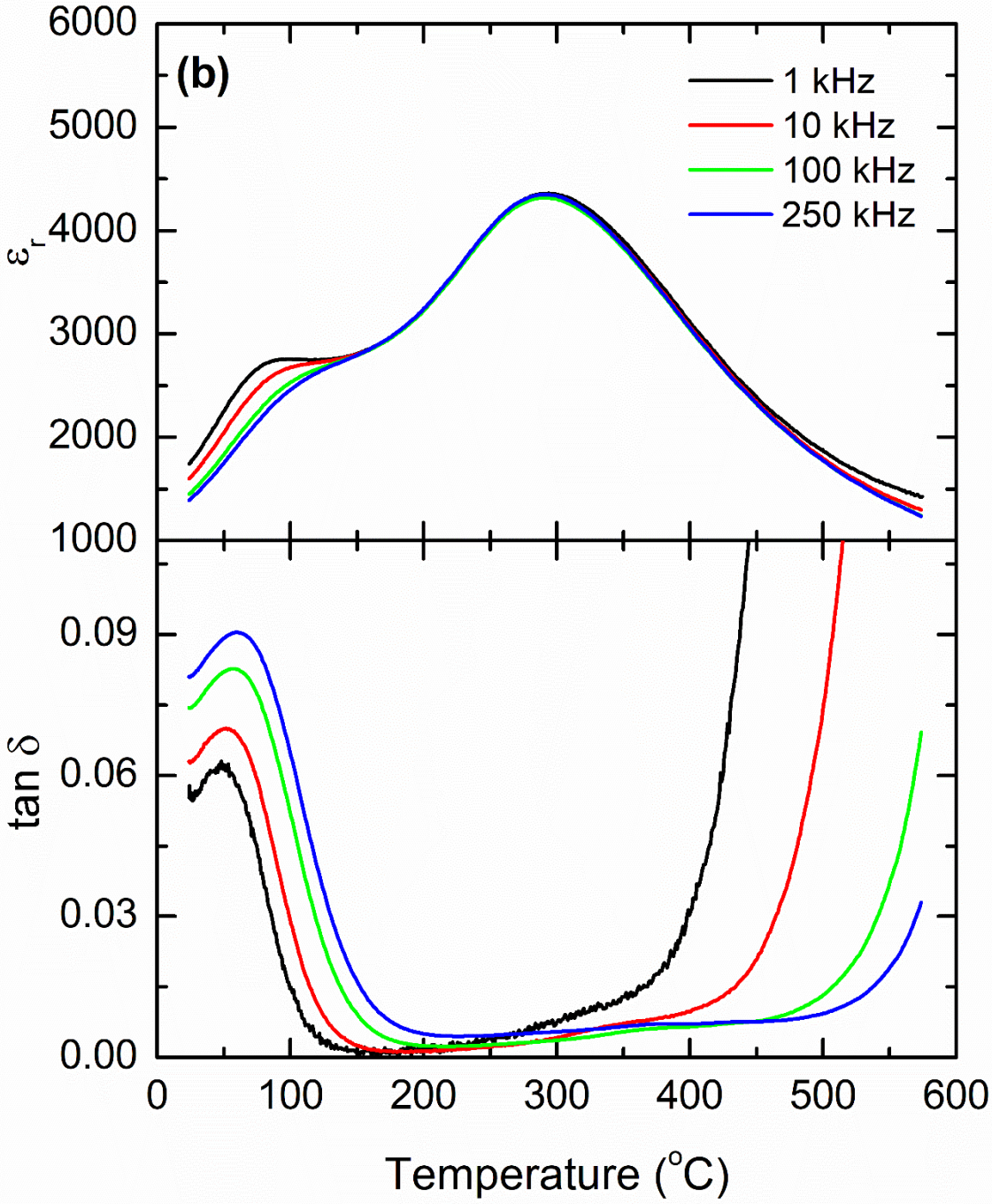
(b)
1 kHz
10 kHz
100 kHz
250 kHz
ε_r
6000
5000
4000
3000
2000
1000
tan δ
0.09
0.06
0.03
0.00
0
100
200
300
400
500
600
Temperature (°C)

Fig5b

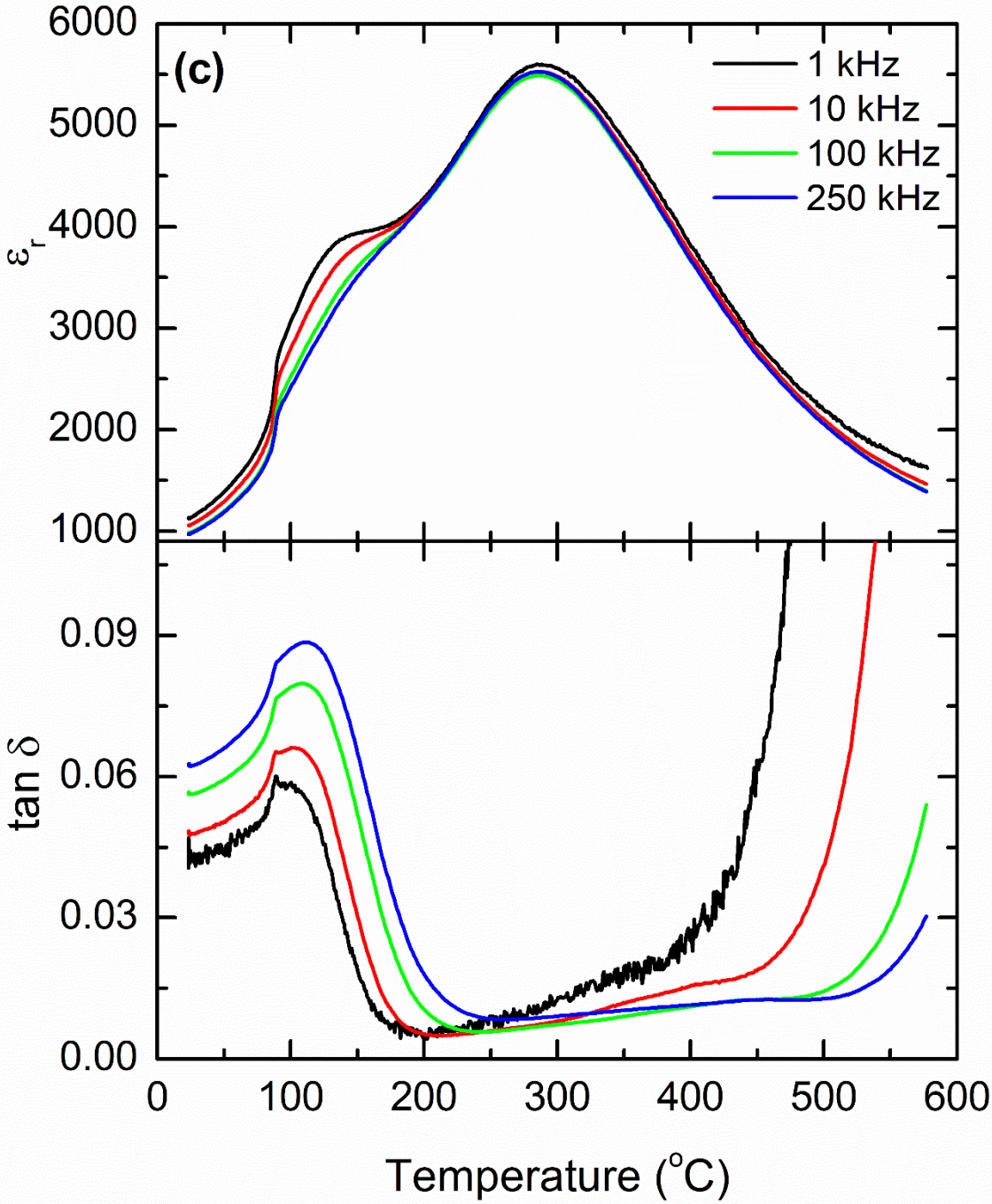
(c)
1 kHz
10 kHz
100 kHz
250 kHz
ε_r
6000
5000
4000
3000
2000
1000
tan δ
0.09
0.06
0.03
0.00
0
100
200
300
400
500
600
Temperature (°C)

Fig5c

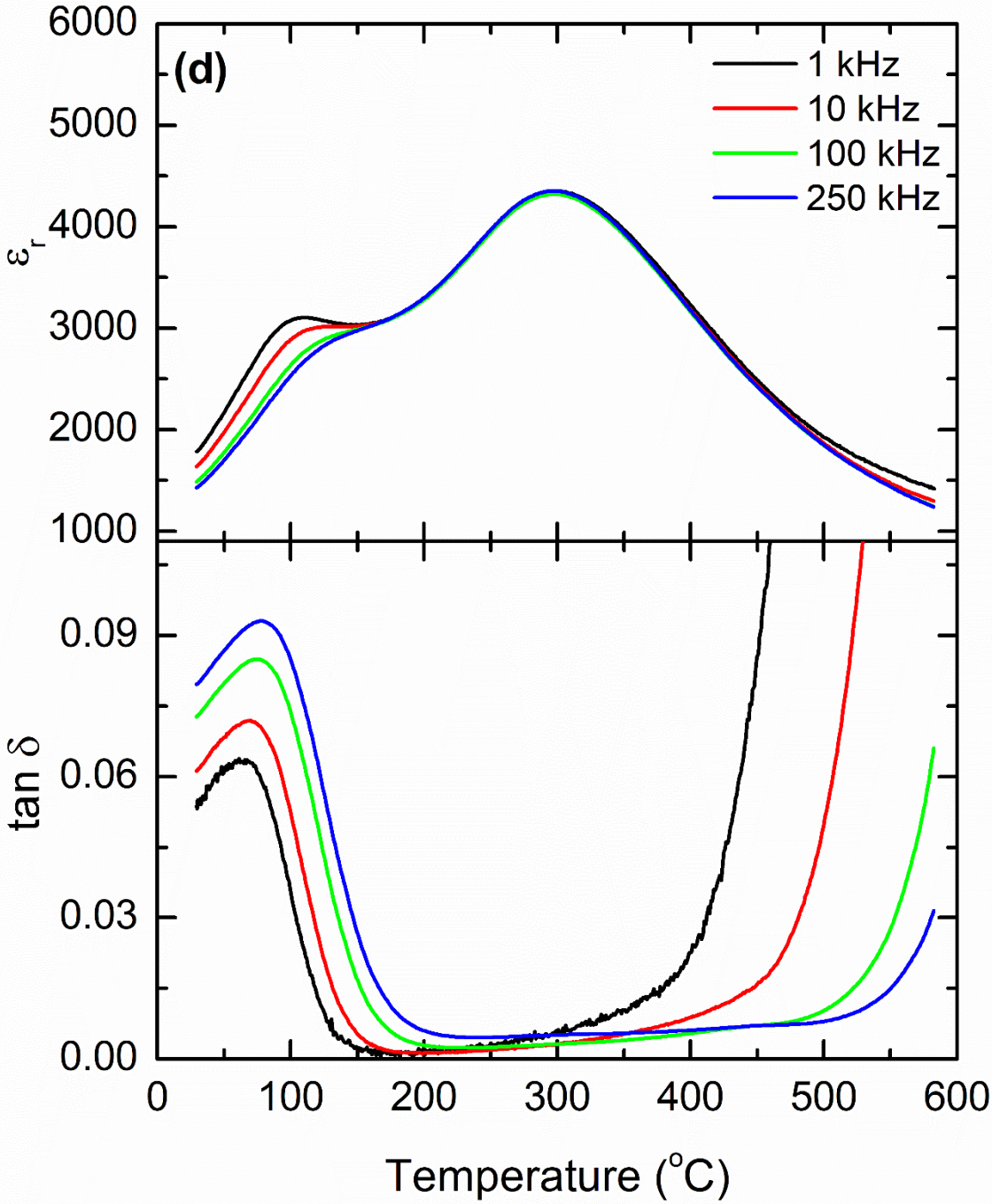
(d)
1 kHz
10 kHz
100 kHz
250 kHz
ε_r
6000
5000
4000
3000
2000
1000
tan δ
0.09
0.06
0.03
0.00
0
100
200
300
400
500
600
Temperature (°C)

Fig5d

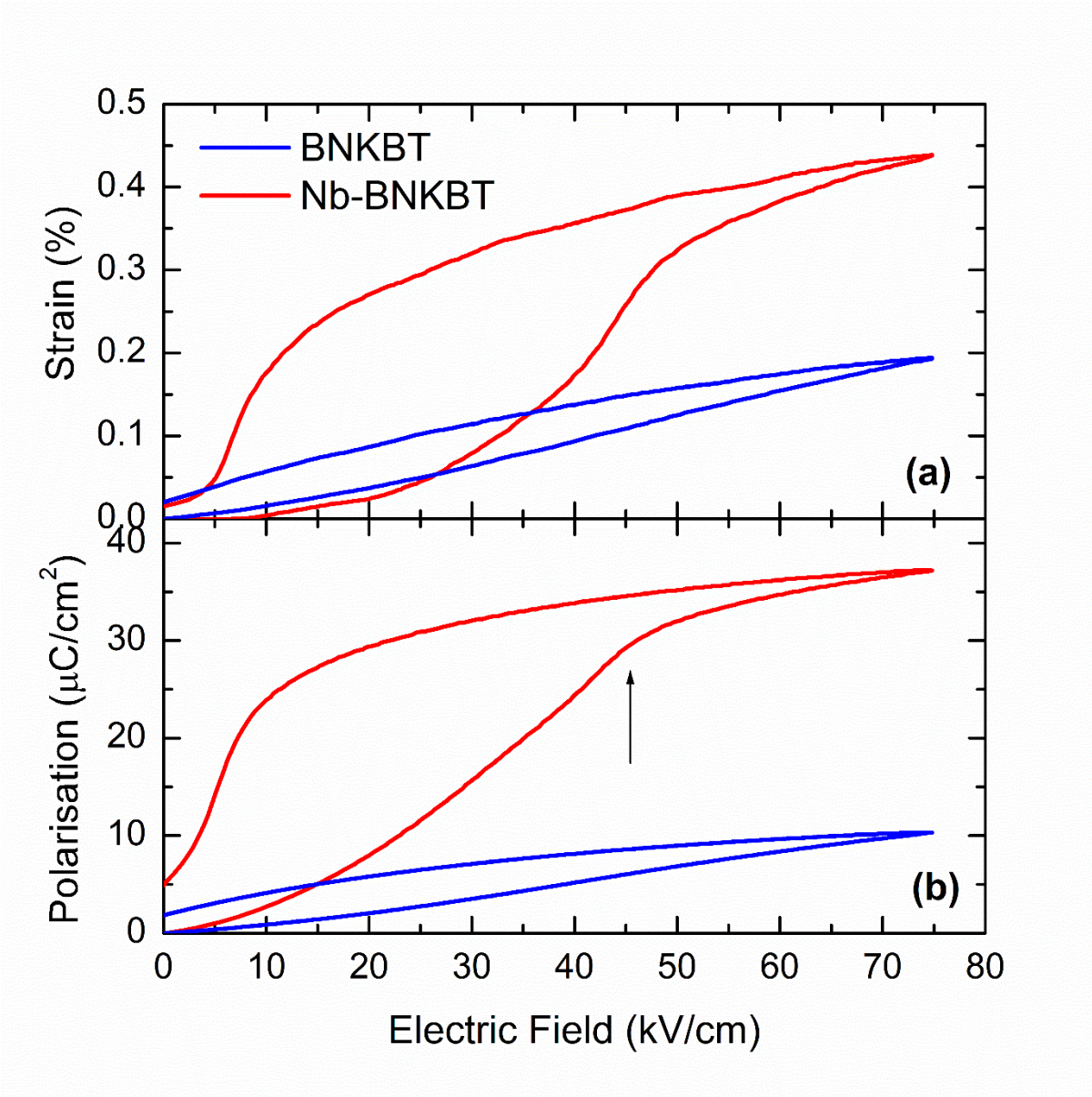
BNKBT
Nb-BNKBT
Strain (%)
0.5
0.4
0.3
0.2
0.1
0.0
(a)
Polarisation (μC/cm²)
40
30
20
10
0
(b)
0
10
20
30
40
50
60
70
80
Electric Field (kV/cm)

Fig6

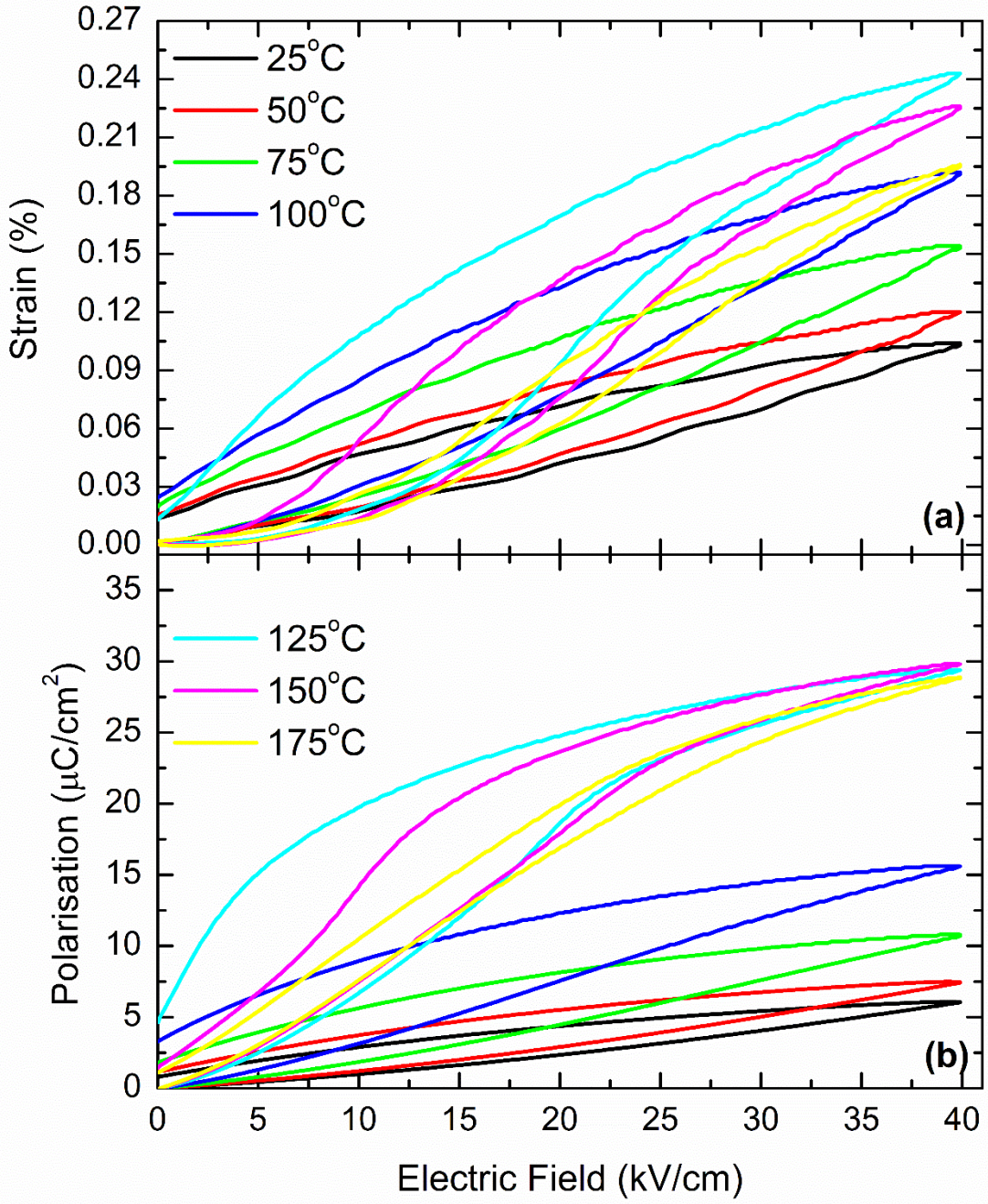
Strain (%)
0.27
0.24
0.21
0.18
0.15
0.12
0.09
0.06
0.03
0.00
25°C
50°C
75°C
100°C
(a)
Polarisation (μC/cm²)
35
30
25
20
15
10
5
0
125°C
150°C
175°C
(b)
0
5
10
15
20
25
30
35
40
Electric Field (kV/cm)

Fig7a,b

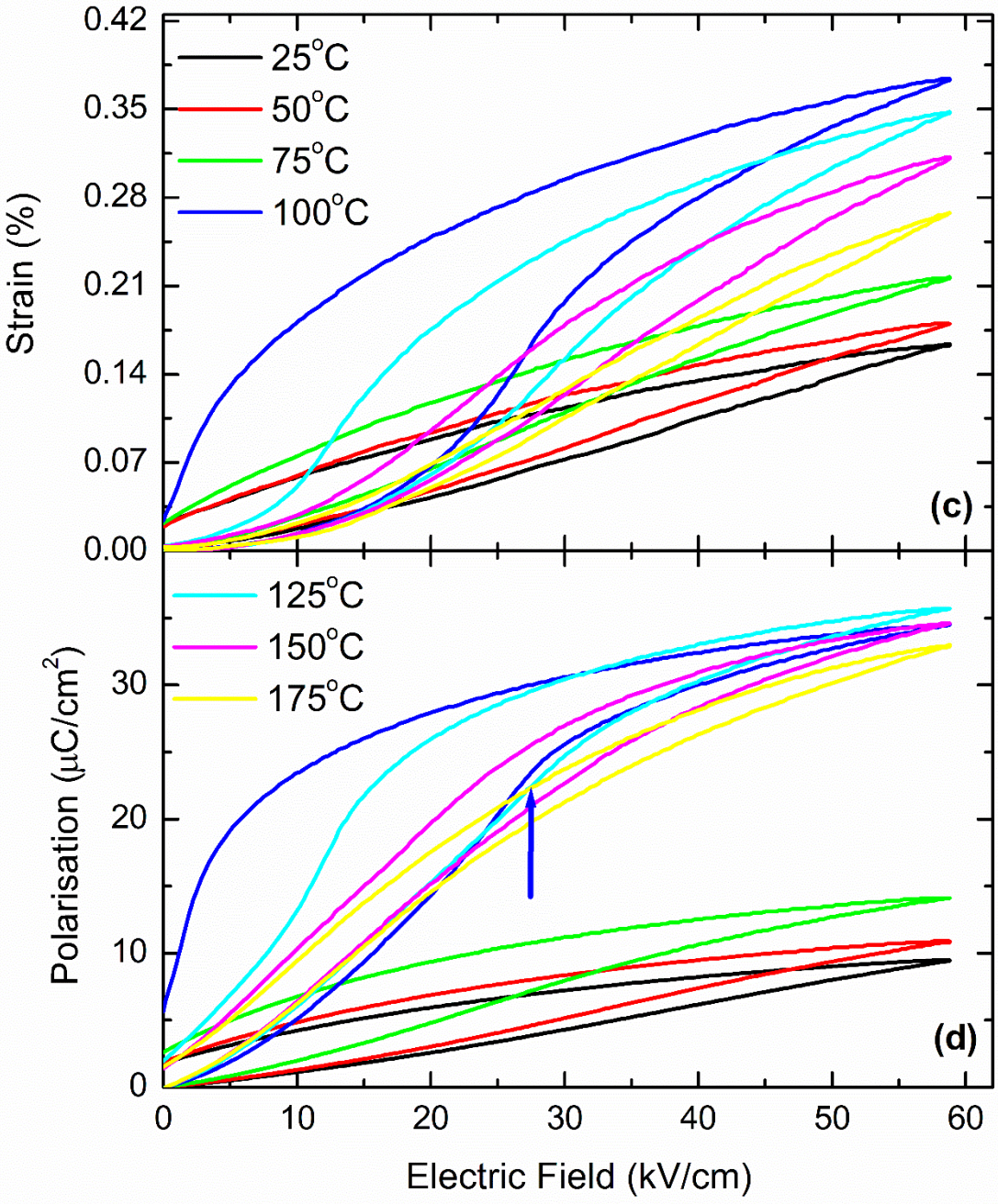
0.42
0.35
0.28
0.21
0.14
0.07
0.00
Strain (%)
25°C
50°C
75°C
100°C
(c)
125°C
150°C
175°C
Polarisation (μC/cm²)
30
20
10
0
(d)
0
10
20
30
40
50
60
Electric Field (kV/cm)

Fig7c,d

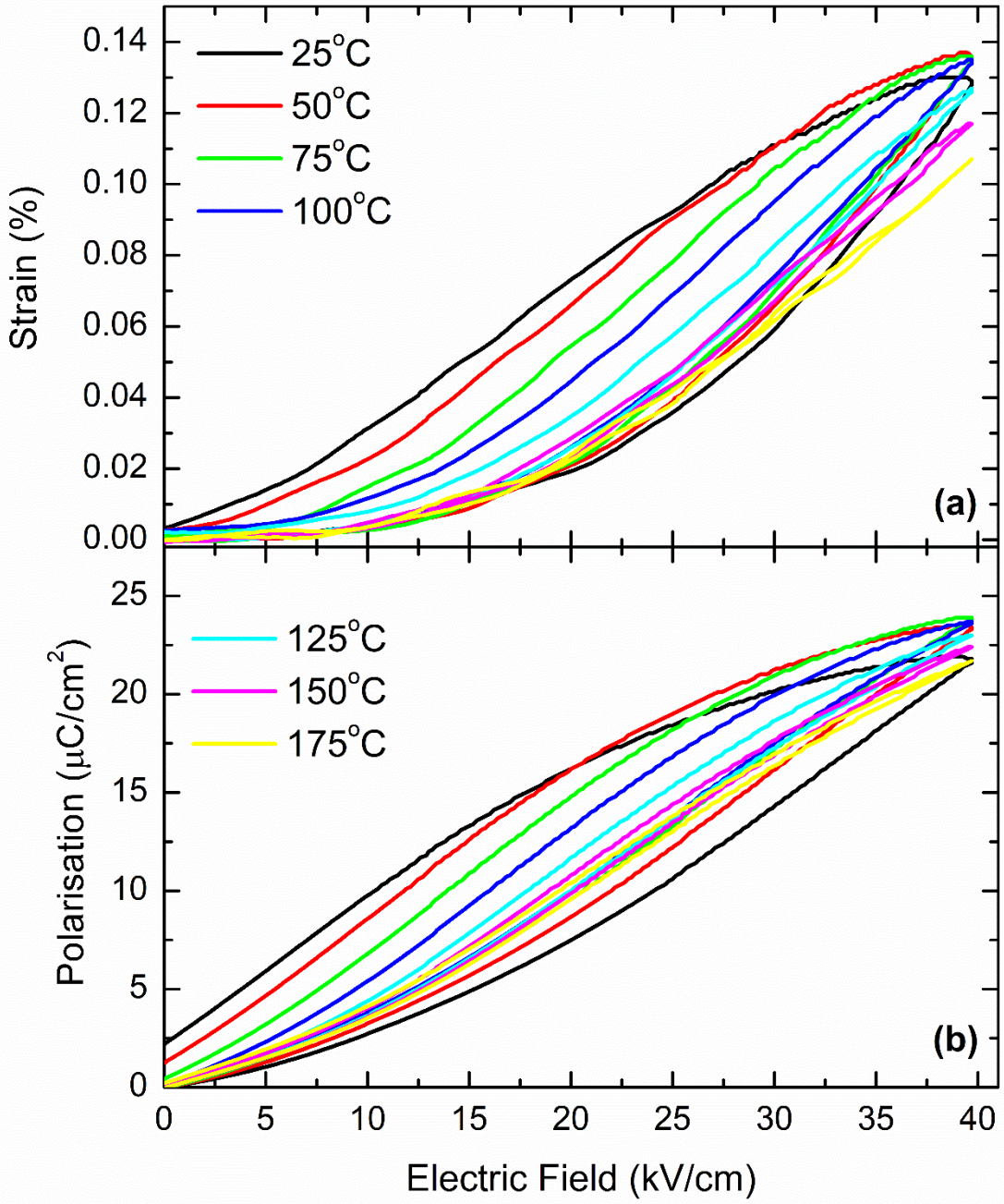
0.14
0.12
0.10
0.08
0.06
0.04
0.02
0.00
Strain (%)
25°C
50°C
75°C
100°C
(a)
25
20
15
10
5
0
Polarisation (μC/cm²)
125°C
150°C
175°C
(b)
0
5
10
15
20
25
30
35
40
Electric Field (kV/cm)

Fig8a,b

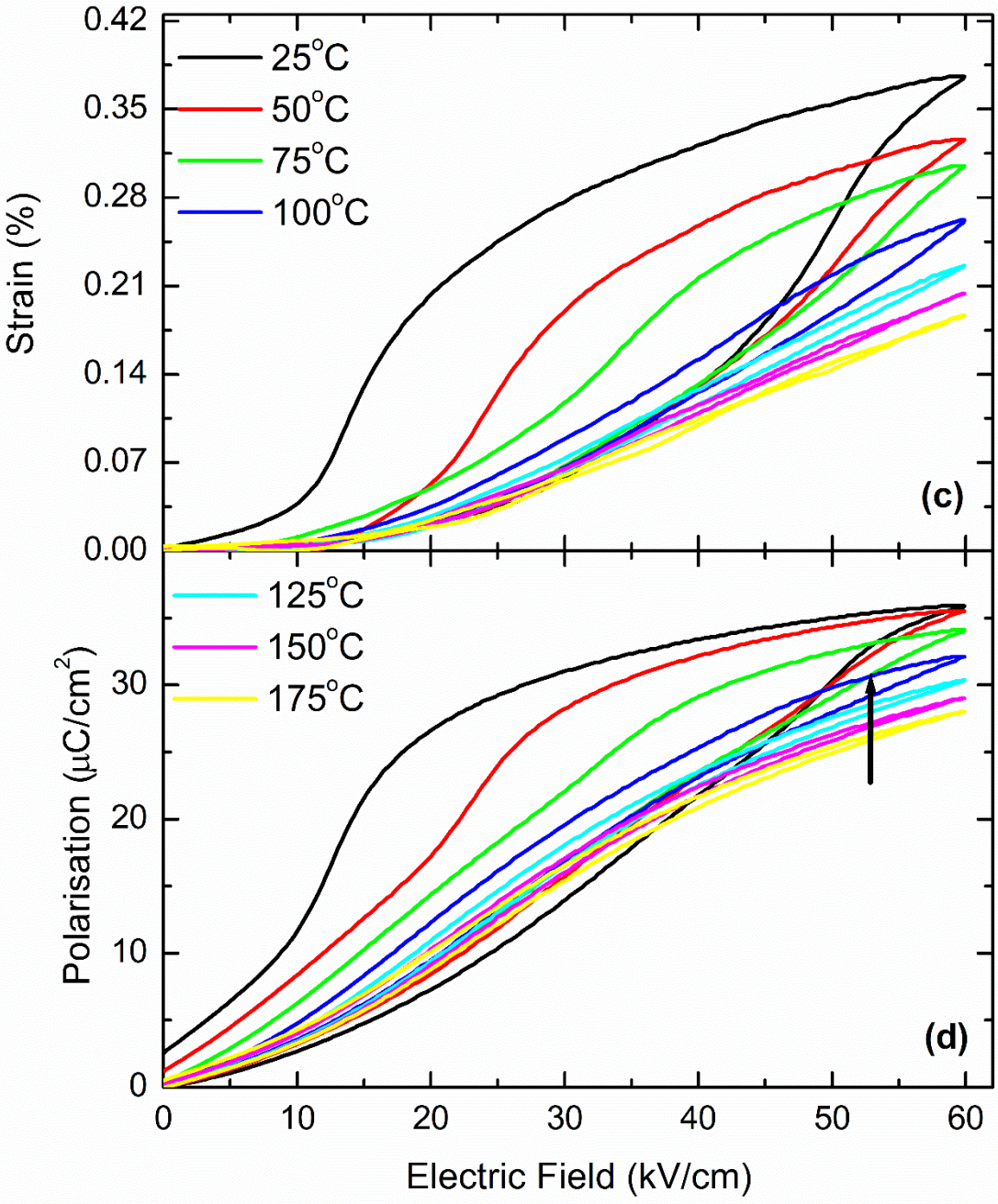
0.42
0.35
0.28
0.21
0.14
0.07
0.00
Strain (%)
25°C
50°C
75°C
100°C
(c)
125°C
150°C
175°C
Polarisation (μC/cm²)
30
20
10
0
(d)
0
10
20
30
40
50
60
Electric Field (kV/cm)

Fig8c,d

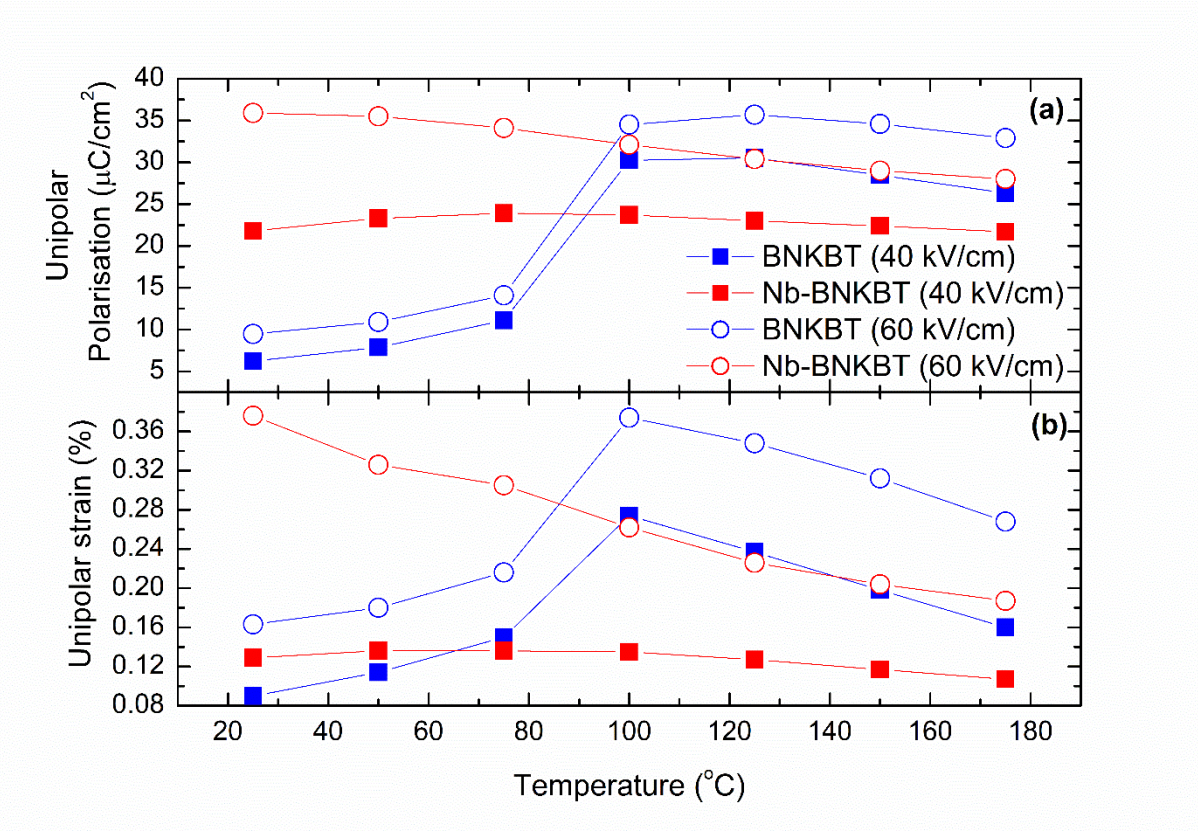
(a)
(b)
Unipolar Polarisation (μC/cm²)
Unipolar strain (%)
Temperature (°C)
BNKBT (40 kV/cm)
Nb-BNKBT (40 kV/cm)
BNKBT (60 kV/cm)
Nb-BNKBT (60 kV/cm)

Fig9

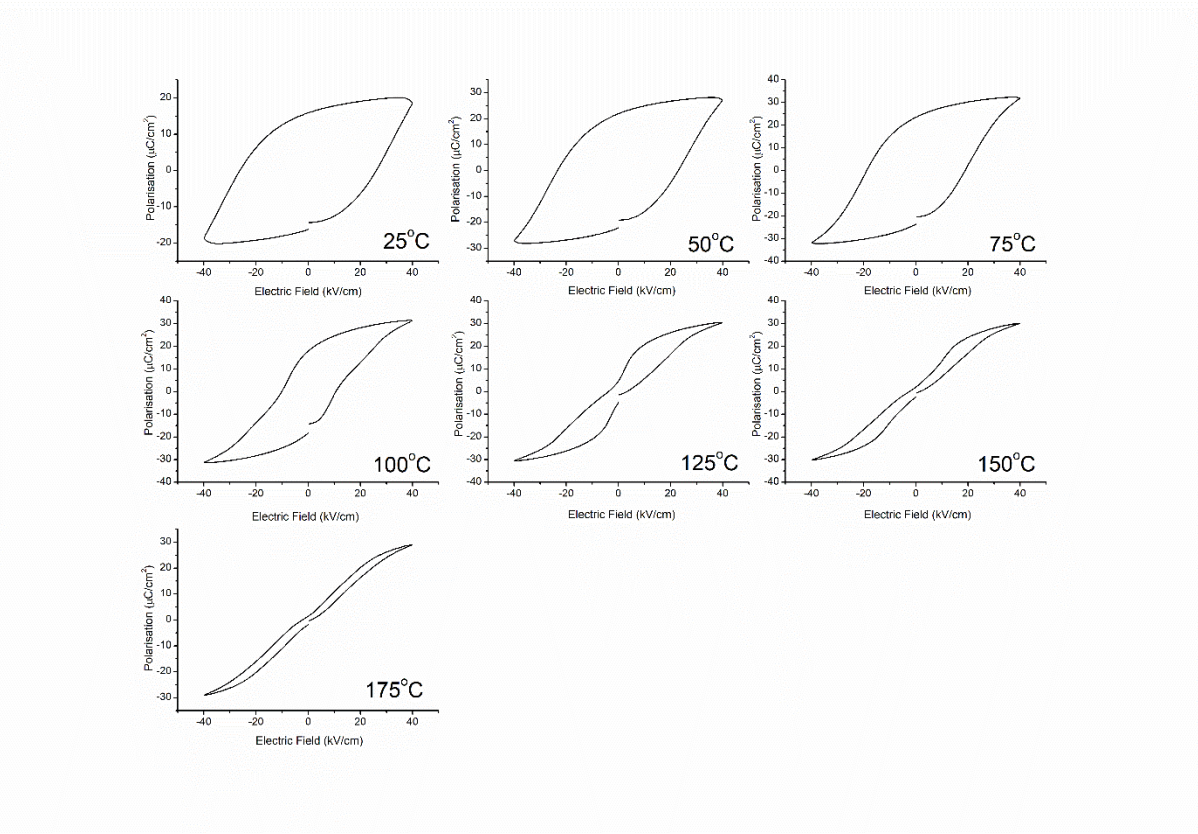
25°C
50°C
75°C
100°C
125°C
150°C
175°C
Polarisation (μC/cm²)
Electric Field (kV/cm)

Fig S1a

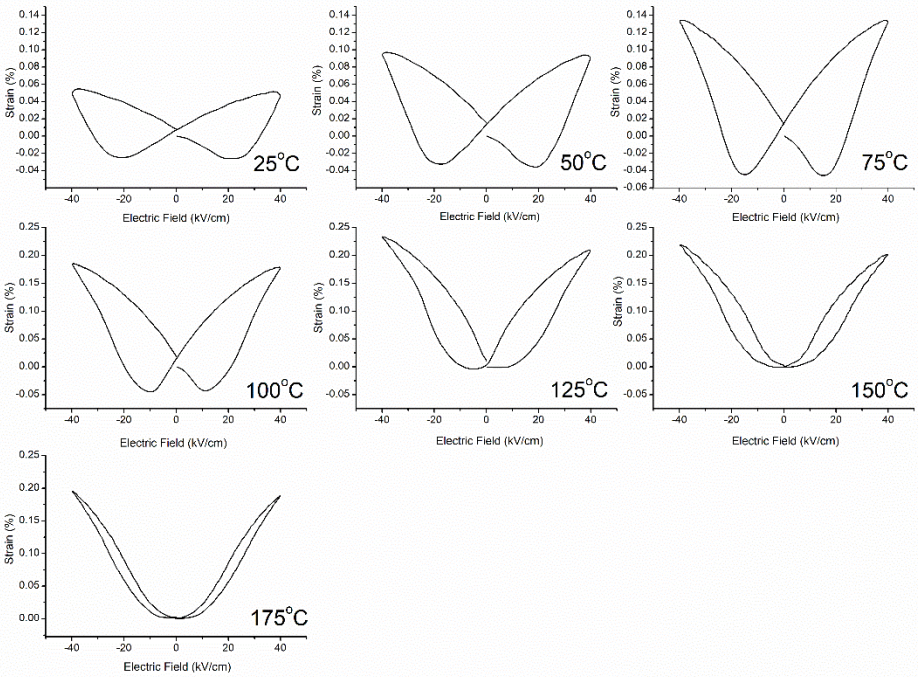

Fig S1b

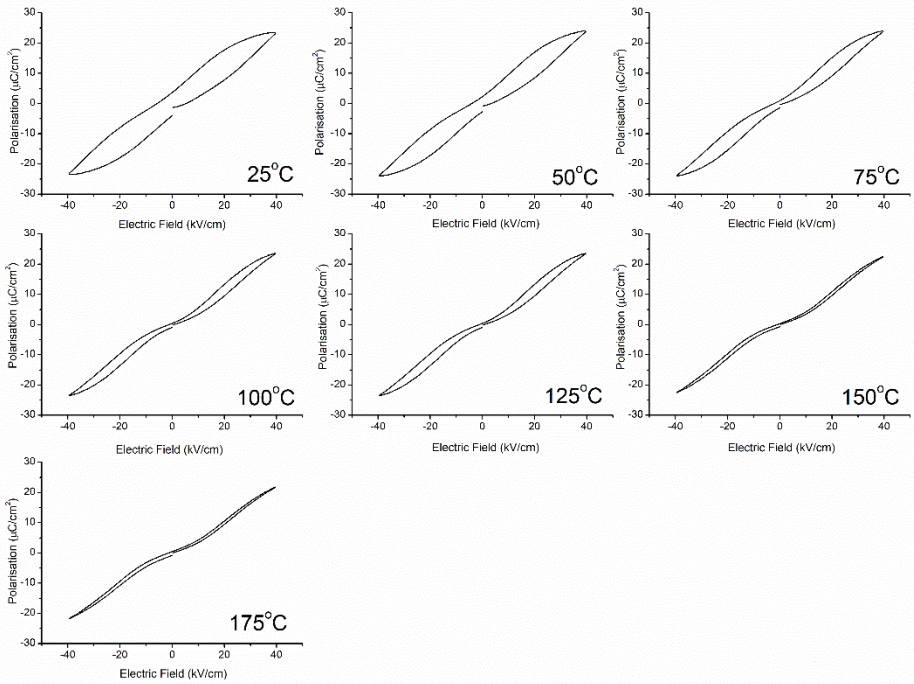

Fi S2a

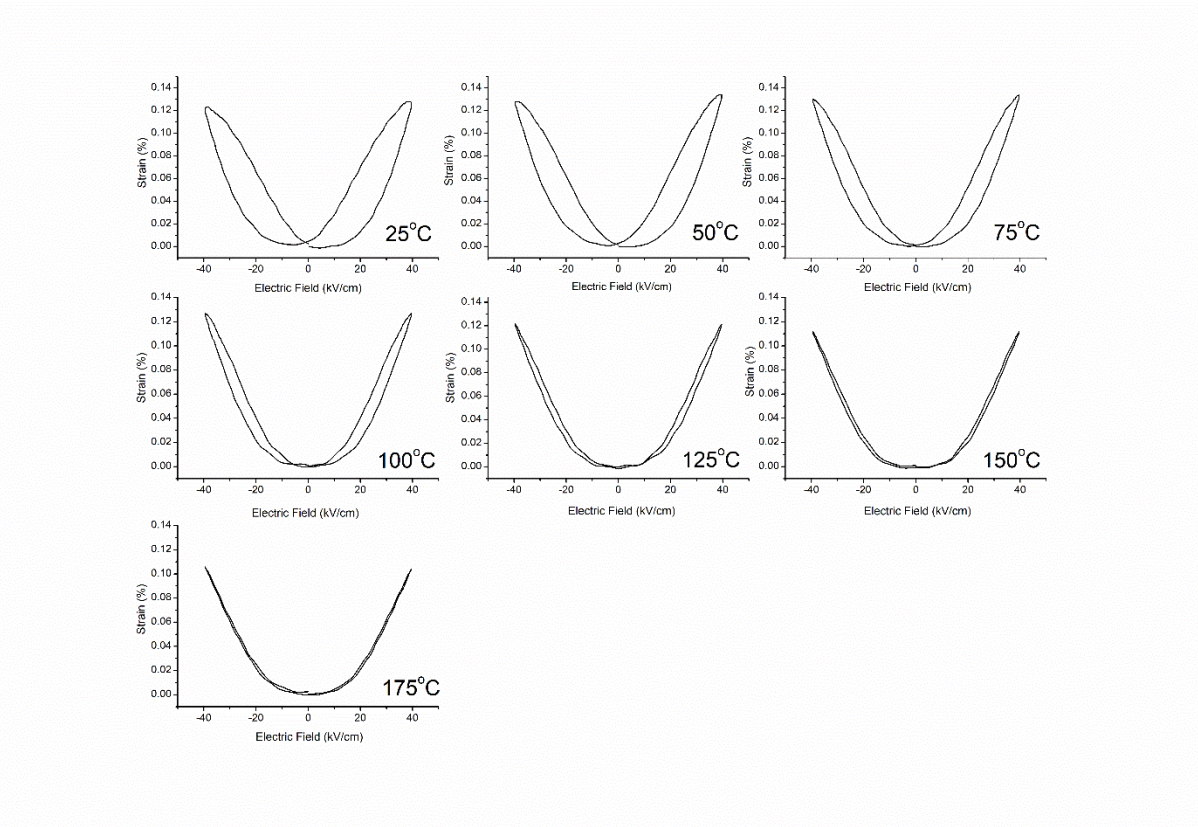
25°C
50°C
75°C
100°C
125°C
150°C
175°C
Strain (%)
Electric Field (kV/cm)

FigS2b

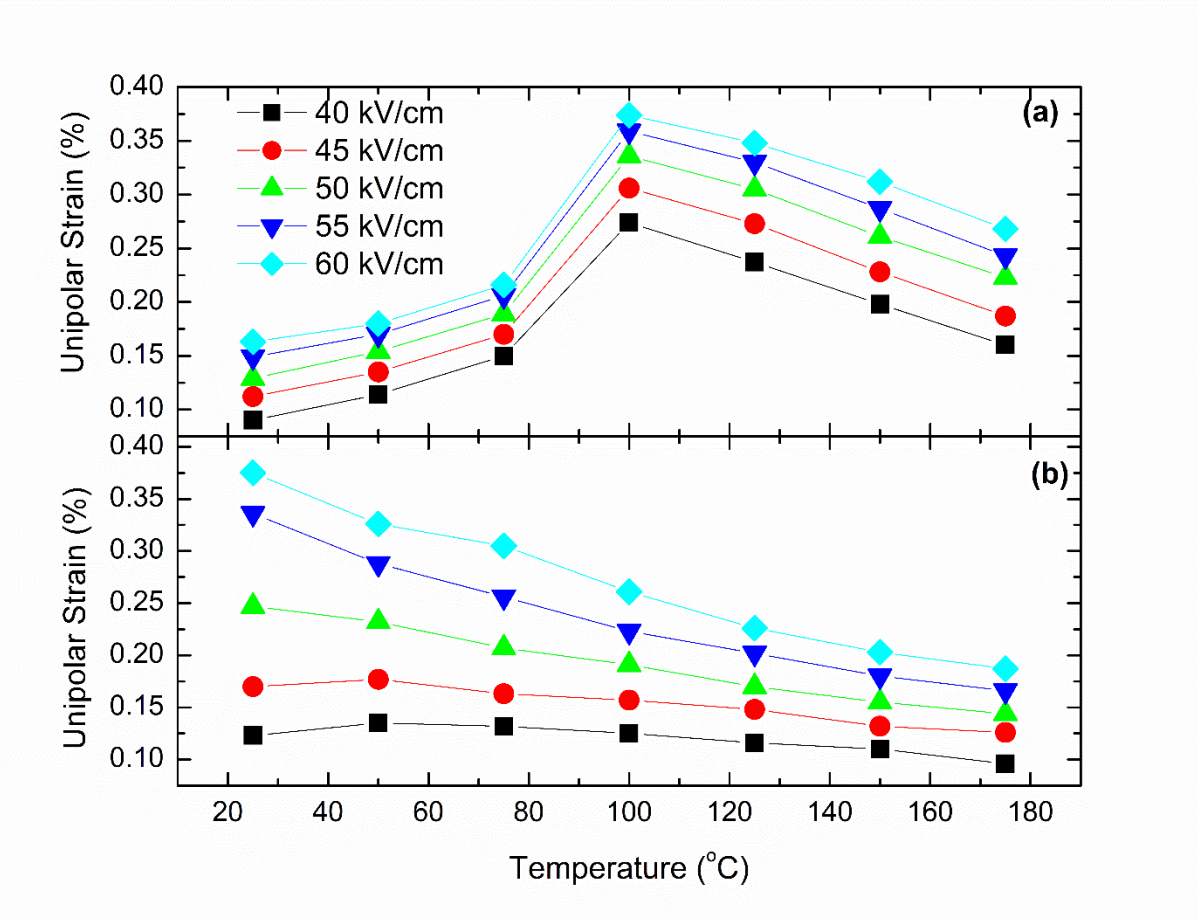
40 kV/cm
45 kV/cm
50 kV/cm
55 kV/cm
60 kV/cm
(a)
(b)
Unipolar Strain (%)
Temperature (°C)

FigS3

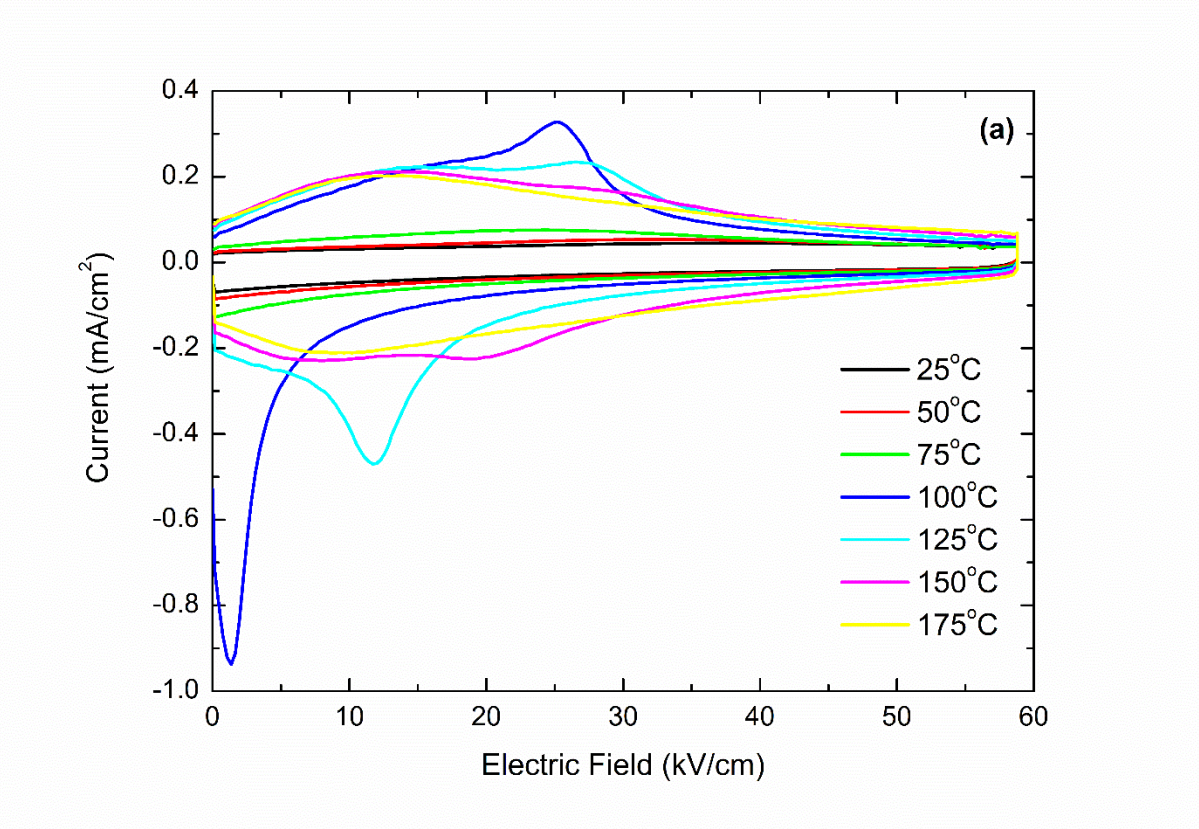

FigS4a

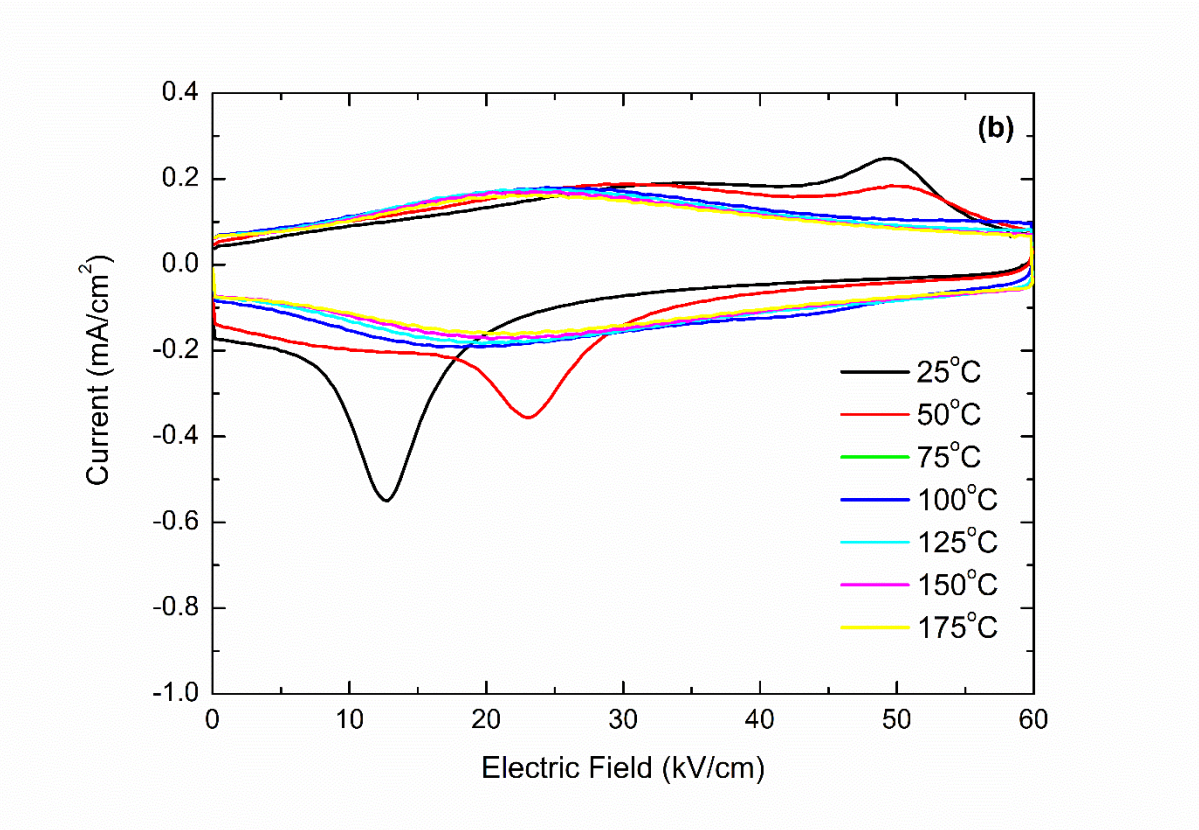

FigS4b